AFRL-RZ-WP-TR-2010-2026

TURBOMACHINERY FLUID MECHANICS AND CONTROL

Steven L. Puterbaugh, David Car, and S. Todd Bailie

Compressor Aero Research Laboratory
Fan and Compressor Branch

JANUARY 2010
Final Report

AIR FORCE RESEARCH LABORATORY
PROPULSION DIRECTORATE
WRIGHT-PATTERSON AIR FORCE BASE, OH 45433-7251
AIR FORCE MATERIEL COMMAND
UNITED STATES AIR FORCE

NOTICE AND SIGNATURE PAGE

Using Government drawings, specifications, or other data included in this document for any purpose other than Government procurement does not in any way obligate the U.S. Government. The fact that the Government formulated or supplied the drawings, specifications, or other data does not license the holder or any other person or corporation; or convey any rights or permission to manufacture, use, or sell any patented invention that may relate to them.

This report was cleared for public release by the USAF 88th Air Base Wing (88 ABW) Public Affairs Office (PAO) and is available to the general public, including foreign nationals. Copies may be obtained from the Defense Technical Information Center (DTIC) (http://www.dtic.mil).

AFRL-RZ-WP-TR-2010-2026 HAS BEEN REVIEWED AND IS APPROVED FOR PUBLICATION IN ACCORDANCE WITH ASSIGNED DISTRIBUTION STATEMENT.

*//Signature//

STEVEN L. PUTERBAUGH
Compressor Aero Research Lab
Fan and Compressor Branch

//Signature//

WILLIAM W. COPENHAVER
Acting Branch Chief
Fan and Compressor Branch

*//Signature//

ROBERT D. HANCOCK
Principal Scientist
Turbine Engine Division

This report is published in the interest of scientific and technical information exchange and its publication does not constitute the Government's approval or disapproval of its ideas or findings.

*Disseminated copies will show "//Signature//" stamped or typed above the signature blocks.

REPORT DOCUMENTATION PAGE

Form Approved
OMB No. 0704-0188

1. REPORT DATE *(DD-MM-YY)*	2. REPORT TYPE	3. DATES COVERED *(From - To)*
January 2010	Final	01 January 2002 – 30 September 2009

4. TITLE AND SUBTITLE
TURBOMACHINERY FLUID MECHANICS AND CONTROL

5a. CONTRACT NUMBER
IN HOUSE

5b. GRANT NUMBER

5c. PROGRAM ELEMENT NUMBER
61102F

6. AUTHOR(S)
Steven L. Puterbaugh, David Car, and S. Todd Bailie

5d. PROJECT NUMBER
2307

5e. TASK NUMBER
S1

5f. WORK UNIT NUMBER
2307S128

7. PERFORMING ORGANIZATION NAME(S) AND ADDRESS(ES)

Compressor Aero Research Laboratory, Fan and Compressor Branch (AFRL/RZTF)
Air Force Research Laboratory, Propulsion Directorate
Wright-Patterson Air Force Base, OH 45433-7251
Air Force Materiel Command
United States Air Force

8. PERFORMING ORGANIZATION REPORT NUMBER
AFRL-RZ-WP-TR-2010-2026

9. SPONSORING/MONITORING AGENCY NAME(S) AND ADDRESS(ES)

Air Force Research Laboratory
Propulsion Directorate
Wright-Patterson Air Force Base, OH 45433-7251
Air Force Materiel Command
United States Air Force

10. SPONSORING/MONITORING AGENCY ACRONYM(S)
AFRL/RZTF

11. SPONSORING/MONITORING AGENCY REPORT NUMBER(S)
AFRL-RZ-WP-TR-2009-2026

12. DISTRIBUTION/AVAILABILITY STATEMENT
Approved for public release; distribution unlimited.

13. SUPPLEMENTARY NOTES
PAO Case Number: 88ABW-2010-0241; Clearance Date: 22 January 2010.

14. ABSTRACT
Slot jet flow control concepts were developed and explored for the application to axial compressor stators. The concepts were demonstrated in a high speed wind tunnel to simulate a highly loaded stator passage. The midspan boundary layer flow could be forced to attach most effectively with addition of streamwise vorticity (vortex generators and discrete jets) however the endwalls continue to be poorly behaved until large fractions of the overall flow were passed through the slot jet.

15. SUBJECT TERMS
Axial compressor, flow control, compressor stator

16. SECURITY CLASSIFICATION OF:			17. LIMITATION OF ABSTRACT:	18. NUMBER OF PAGES	19a. NAME OF RESPONSIBLE PERSON (Monitor)
a. REPORT	b. ABSTRACT	c. THIS PAGE			Steven L. Puterbaugh
Unclassified	Unclassified	Unclassified	SAR	52	19b. TELEPHONE NUMBER *(Include Area Code)* (937) 255-7432

Standard Form 298 (Rev. 8-98)
Prescribed by ANSI Std. Z39-18

TABLE OF CONTENTS

SECTION **Page**

LIST OF FIGURES

Page

1.0 INTRODUCTION

The Turbine Engine Division of the Propulsion Directorate at AFRL has established a technology program called the Versatile Affordable Advanced Turbine Engine (VAATE) program in which compression system technology development can play a significant part. The compression system contribution to the VAATE program goals will be decreased weight for a given performance level, increased efficiency, and reduced parts count among other cost-related items. Reducing the number of stages for a given pressure ratio, i.e. increased stage loading reduces weight by reducing length. Length and therefore weight can also be reduced by decreasing the axial distance between blade rows. Reduced axial spacing can also have an efficiency contribution. Further, a parts count reduction may by realized by a reduction in the number of stages. The Fan and Compressor Branch established a 6.2-funded in-house research program to address these areas of need. The high-level objective of this program was to develop and transition technologies that make unprecedented loading levels possible. A specific loading level with an implied efficiency was targeted for the program as shown in Figure 1.

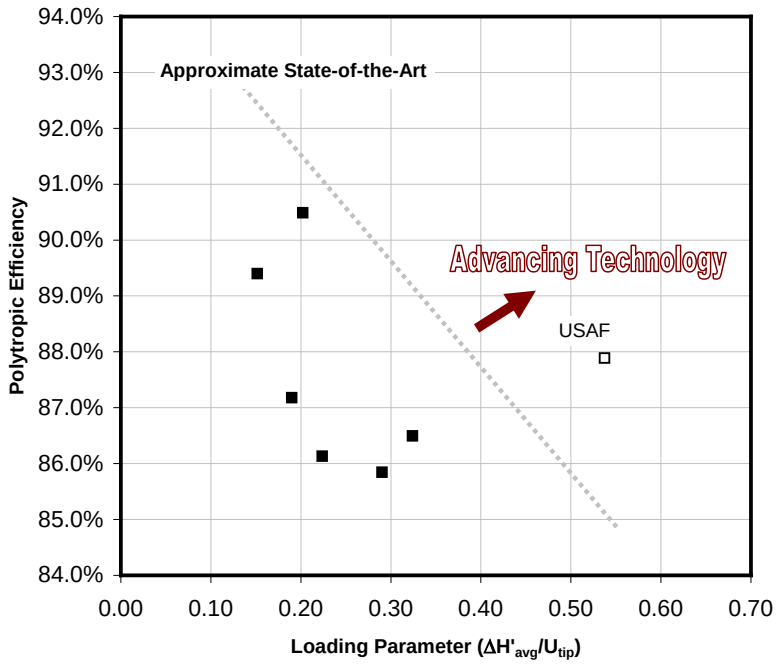

Figure 1: Compression system stage loading technology

This program was comprised of efforts funded by both 6.1 and 6.2 sources – the work included in this report was funded by 6.1 (AFOSR). Fundamental research funded by

AFOSR was intended to provide the theoretical framework to move forward with technologies exploited by 6.2 efforts.

It is anticipated that a practical compression system operating at the very high loading levels implied by the target described above will require boundary layer control to achieve the associated diffusion requirements. The subject effort pursued basic research in this area to accomplish the following: 1) understand physical phenomena limiting diffusion potential in turbomachinery, 2) identify modeling deficiencies (both model adequacy and application) for boundary layers in a strong adverse pressure gradient, 3) develop and demonstrate flow control concepts, and 4) develop design guidelines for flow control applications.

2.0 BACKGROUND

The term high loading for compression system performance implies high diffusion rates within its rotor and stator blade rows. By aerodynamic necessity, as diffusion rates are increased, boundary layers become thick and tend toward separation. A useful compression system will not have excessively large areas of boundary layer separation due to the associated reduction in efficiency and stall margin. The development of highly loaded compression systems then must include the development of approaches which extend stable operation (i.e. suppress separation) into regimes which would break down under ordinary circumstances.

Flow control, defined here as technologies which directly influence the boundary layer, has the potential of extending flow field stability beyond that which is typical. Flow control in external aerodynamics, such as on wings, has been investigated since the 1970's. However, flow control particular to axial compression systems has become a very active research topic only in the last decade [1–4]. It has the potential to open the design envelope for axial compressors to higher loading levels. This translates into higher overall pressure ratios for reduced thrust specific fuel consumption. Increased loading also increase thrust-to-weight ratio by reducing turbine engine axial length for a given pressure ratio.

Both the rotor and stator blade rows in an axial turbomachine diffuse their respective incoming flow fields. Therefore flow control technologies are equally desirable in each. However, since the application of flow control to a rotor requires the extra complexity of bridging stationary to rotating hardware, the decision was made to concentrate flow control development efforts here on the stator. The fundamental physics remain the same in both cases, but are much more efficiently investigated in the stator blade row.

The blade rows in axial turbomachines are most accurately characterized as curved, quasi-two-dimensional diffusers. As such, two-dimensional boundary layer separation can occur on the blade surfaces (most often on the suction surface), and three-dimensional boundary layer separation can occur at the blade corners and endwalls. The resulting flowfield, particularly for highly loaded blade rows, can be very complex and requires systematic study. In the work described here, experimental, computational, and analytical methods were used to investigate approaches to manage the health of the boundary layers in this environment. Specific objectives were as follows: 1) Characterize co-flow inset jets, co-flow linear and tailored jets, and discrete jets used for flow control. Quantify the flow control diffusion enhancement capacity as it relates to important blade row geometric and fluid mechanics characteristics. These include streamwise diffusion rates, wall curvature effects, potential field effects due to adjacent vanes, and position and size of the flow control device. Determine the functional relationship between the appropriate dimensionless groups. In particular, determine the relationship between diffusion capacity and energy input by the secondary flow stream. 2) Develop modeling and design approaches for compression system flow control. Develop design and design optimization strategies that integrate the effect of flow control. Develop phenomenological descriptive models that provide the designer insight into how to best exploit AFC and that can be incorporated into turbomachinery design systems. 3) Determine system impacts. Develop a generic approach to determine the thermodynamic limits of a flow control-enhanced compression system. Perform system studies for the concepts under consideration.

This effort underpins the Fan and Compressor Branch 6.2 research program with the fundamental research required to successfully apply flow control for diffusion enhancement. The approach here is to develop concepts first through analysis, through numerical simulation, through simplified experiments, and finally through subscale compression system demonstration.

3.0 TECHNICAL APPROACH

3.1 Experimental Apparatus

A small scale, bench top device was developed to investigate the flow control concepts in a fundamental fashion. A convergent/divergent wind tunnel having the capability of modifying diffusion levels developed. The divergent section consisted of two curved wall sections similar to a cascade passage. This tunnel provided an inexpensive and simple experimental setup that was used to take very detailed total pressure and Digital Particle Image Velocimetry (DPIV) measurements of the flow control diffusion process

and provided a test bed for the design of a flow delivery system. The wind tunnel was 2D in nature with an approximate 8:1 aspect ratio at the throat. The issues to address include: 1) the role of irreversibility in the flow control process and what processes are the significant contributors, 2) evaluation of the flow control configurations, 3) quantify the flow control diffusion enhancement capacity as it relates to important blade row geometric and fluid mechanics characteristics (these include streamwise diffusion rates, wall curvature effects, potential field effects due to adjacent vanes, and position and size of the inset cavity), and 4) determine the functional relationship between the appropriate dimensionless groups (in particular, determine the relationship between diffusion capacity and energy input by the secondary flow stream). A schematic of the device is shown in Figure 2.

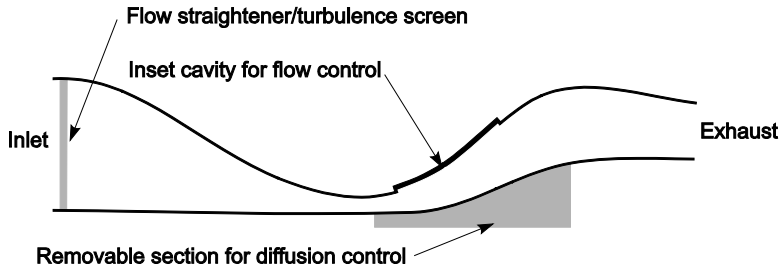

Figure 2: Schematic of the flow control experimental apparatus

The tunnel was driven by an automotive supercharger driven by a 50 HP electric motor which provides 0.7 Mach flow at the entrance to the diffuser section. The diffuser simulates a stator performing at a diffusion factor of 0.7. The device was an atmospheric in-draft design. After passing through a bellmouth and flow straightener, the airflow accelerates through a converging inlet of roughly 12:1 area contraction to a rectangular throat, 1.5 x 10.2 cm (0.6 x 4.0 in). The throat, typically operated at Mach 0.7, is the beginning of the curved diffuser test section. The diffuser geometry was based on aggressive goals for an axial compression system. The diffuser passage has an exit-to-throat area ratio of 2.92, a flow turning angle of 70 degrees, with suction (convex) side radius of curvature nearly constant at 5.1 cm (2.0 in). Following the diffuser is a sudden expansion into a rectangular settling chamber. An adaptor piece guided the flow from the settling chamber into a flexible 7.6 cm (3 in) diameter duct connected to the primary flow driver. Figure 3 illustrates the basic flowpath from the inlet (at right) to the dump chamber (left).

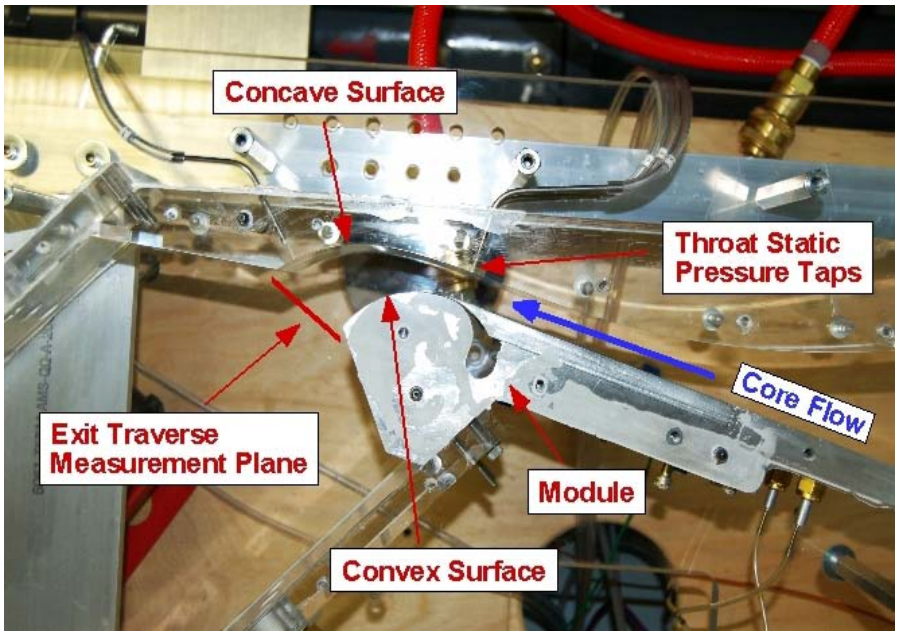

Figure 3: Test section of wind tunnel used to simulate a stator passage

Figure 4 shows a side view of the wind tunnel. Shown is the secondary flow pump (foreground), data acquisition system, and the tunnel (plexiglass section). The entire tunnel could be moved up and down to facility DPIV data acquisition at different spanwise cross sections.

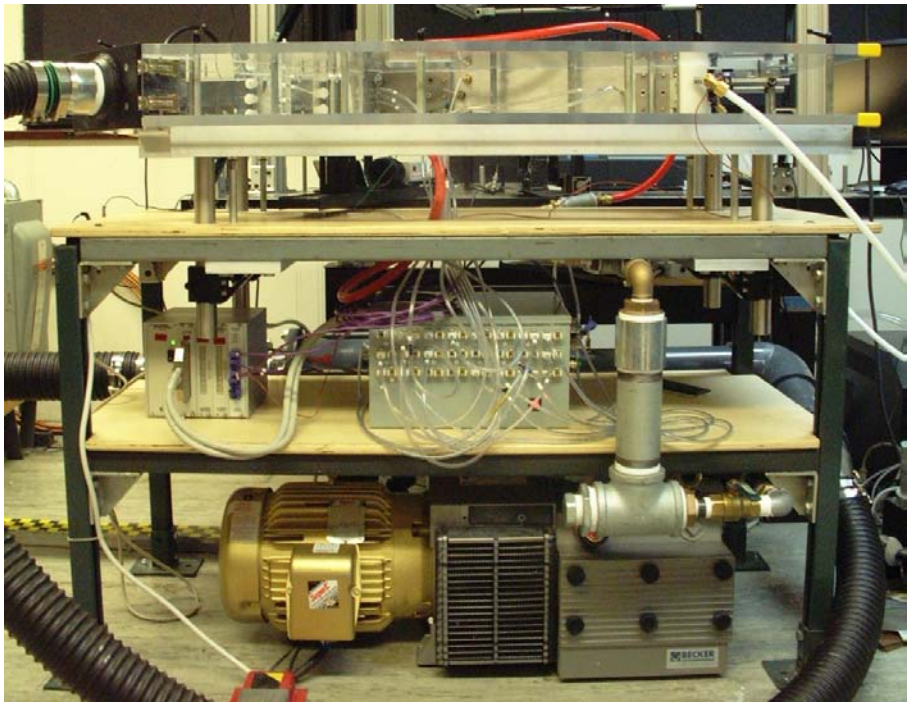

Figure 4: Side view of wind tunnel

Because present research goals include identification of key physical mechanisms relating diffusion and flow control, the tunnel was designed with optical access as a priority. The top and bottom walls are transparent acrylic sheets, and sandwiched in between are wall segments with height of 10.2 cm (4 in). Defining the suction (convex) side of the curved diffuser test section is a readily replaceable aluminum module for testing various flow control concepts. One such module is shown in Figure 5. The planar jet height for these studies was fixed at 0.508 mm and the jet surface was constructed as follows: 1) The baseline convex surface was a constant radius of 50.8 mm ; 2) This radius was reduced 1.397 mm at the throat to accommodate the jet and lip thickness; 3) A linear function in the angular coordinate was used to fit this radius to the 50.8 mm radius at the exit of the passage.

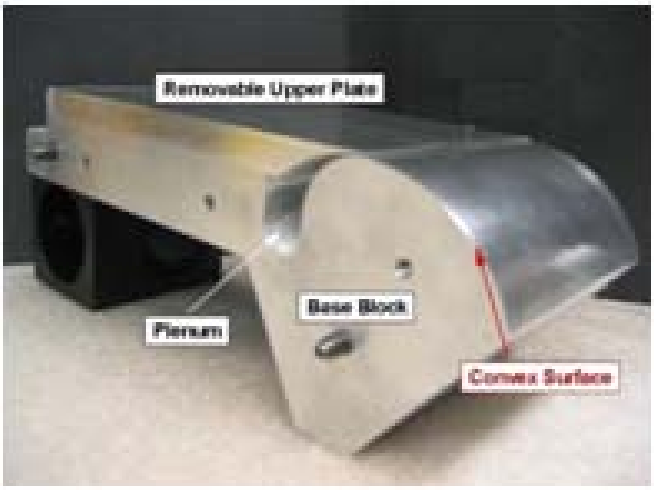

Figure 5: Replaceable flow control module used in wind tunnel test section

3.2 Coflow Inset Jet Theoretical Considerations

The co-flow techniques discussed here were spawned from the work in fluidic vectoring nozzles reported by Prof. Strykowski at the University of Minnesota [5,6,7] and is an attempt to create a similar condition in the stator passage with a re-circulating co-flowing system. One technique in the fluidic vectoring of nozzles uses a suction collar that surrounds the exiting jet. This collar is used to create a secondary flow along the collar surface that interacts with the main jet flow, causing the jet flow to be drawn to the collar surface. The mechanism for this vectoring is still under investigation. One of the mechanisms described is a reduction of surface pressure along the collar which causes the main jet to curve toward the collar [7]. Unsteady measurements and simulations also show that a coherent secondary flow structure is not apparent along the collar surface [5,6], but the secondary flow is highly turbulent. It has been hypothesized that

this interaction between the secondary flow and core jet flow enhances the diffusion process and causes the flow vectoring. It must be noted that the secondary flow in these nozzles is oriented in a counter-flow fashion to the main jet flow, opposite to the co-flowing configuration outlined here for the stator.

For the stator application here, the inset cavity used for “co-flow” blowing encloses a steady re-circulating jet along the suction surface to increase the diffusion characteristics of the passage. This technique imparts no net mass flow change on the core flow and would be supported by a re-circulating secondary flow pumping system. The concept is shown in Figure 6 and Figure 7. The effect is to create an apparent “no-slip” condition along the suction surface, filling the core flow velocity profile and imparting the higher momentum of the jet fluid into the core flow to essentially eliminate boundary layer separation. A computational study in which this approach has been applied to an ultra high turning cascade section has demonstrated a diffusion factor of 0.95.

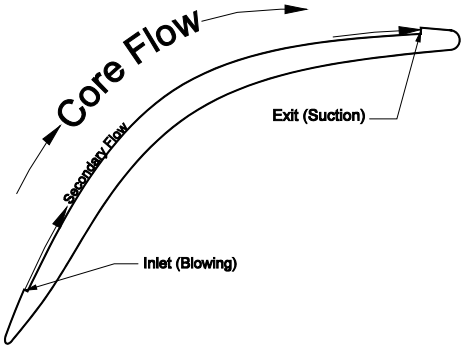

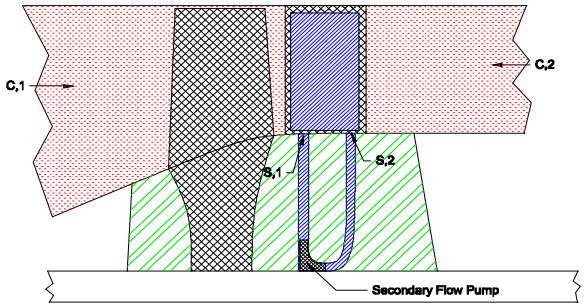

Figure 6: Co-flow control concept **Figure 7: Flow control implementation**

Through the support of the NRC summer faculty program a numerical investigation was begun to consider the potential of sub surface blowing on ultra high diffusion stators. Because of the unusual geometry required to achieve blowing that does not penetrate the stator suction surface plane, a special computational code was required. The concept does not require any of the main core flow to be drawn off for control purposes. Instead, an auxiliary compressor will provide the necessary motive flow for control. Initial computational results were very promising, suggesting that a diffusion factor of 0.95 can be achieved with 70 degrees of turning and only .3% total pressure loss. The “penalty” of this type of arrangement on the overall compression system may not be significant if the required total pressure ratio of the secondary flow system and its efficiency requirement is reasonable. A power and irreversibility analysis was used to address this issue [8].

The system study was separated into 2 parts. The first examined the thermodynamic differences in flow processes that occur for a non-controlled vs. controlled case. The second considered the overall efficiency of a system that included the secondary flow system and its losses. An availability analysis was performed using the simulation results to examine the thermodynamic processes for the two cases. The results revealed that the process associated with the controlled blade produces 50% less loss than the non-controlled blade. This analysis included the irreversibilities that occur in the separation region in the non-controlled case and in the core/jet shear layer region of the controlled case.

In association with cycle analysis personnel within the Propulsion Directorate, an analysis was done using the co-flow flow control technique applied to an extremely highly loaded fan of a notional advanced engine. The fan was single stage, 4.12 pressure ratio, 90% adiabatic efficient rotor, 68° deflection in the stator, and 1.67 stator solidity. The resulting relationship between the secondary flow stream efficiency and the overall efficiency for a fixed overall pressure ratio, rotor efficiency, and isentropic power is shown in Figure 8.

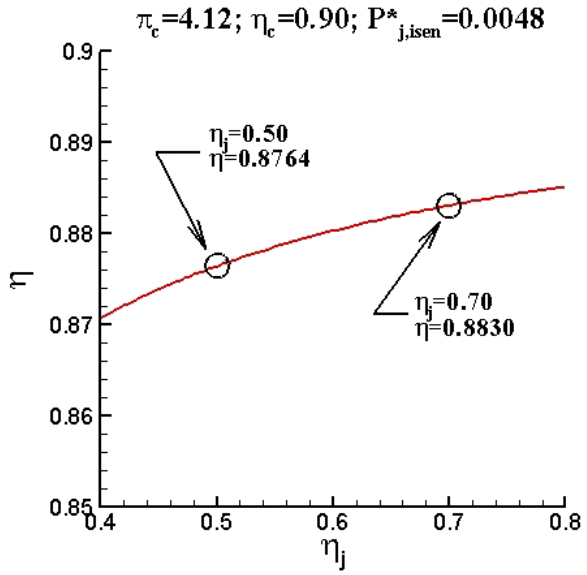

Figure 8: Dependency of overall efficiency on secondary flow system efficiency

A conclusion of the study is that the sensitivity of the overall system efficiency to secondary flow system efficiency is not extremely strong, with the example from the figure showing a 0.66 point difference in overall efficiency for a 20 point difference in secondary system efficiency. For this preliminary study, an engine fuel consumption penalty and a thrust-to-weight benefit were realized with a specific fuel consumption and

thrust-to-weight ratio increase of 1.5% and 3.2% respectively. This was seen as a significant performance improvement that would be applicable to a military fighter engine.

The co-flow configuration using the inset cavity is shown in Figure 9. The cavity was placed on the suction side of the blade in order to maintain an attached boundary layer under a highly adverse pressure gradient.

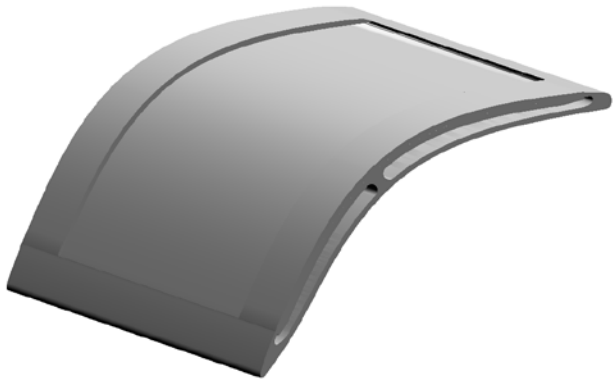

Figure 9: Stator vane with inset cavity

A cascade of airfoils was built and run in the Virginia Tech blow down cascade facility. A 50 hp electric motor and automotive supercharger was used for the secondary flow system. The results from the test were disappointing. Sufficient secondary flow rates were not achieved – particularly for the suction part of the system. It was determined that the internal passages choked on the suction side, thereby limiting the achievable flow. Further numerical studies were completed to improve the flow field performance in the internal passages. It was unclear whether sufficient performance could be achieved on the suction side of the inset cavity. Further work described here concentrated on blowing without the suction part of the device and without the inset cavity. This approach proved much simpler and numerical modeling showed that it provided similar benefits.

3.3 Co-flow Jet Theoretical Considerations – Linear and Tailored Slot Shapes

The co-flow jet concept employed a downstream-facing slot oriented parallel to the leading edge and located near the leading edge on the suction surface of the stator vane. Pressurized air was introduced through this “slot jet” that generated a jet of air parallel to the surface in the streamwise direction that would energize the boundary layer in the highly loaded configuration under investigation. This configuration, called

the “linear slot jet”, became the baseline for the experimental effort utilizing the wind tunnel that simulates a single stator passage.

The stator configuration was designed with a very aggressive implied diffusion rate. This was indicated by the large growth in blockage at the endwalls when flow control was used on the suction surface. This effect will be present in the vane rows in actual compressors.

Machining considerations required the ends of the slot to occur in the side wall/endwall corners. This generated end effects due to the vorticity generated by the changing direction of the shear layer as the end was approached. Work by Visbal et al. [9] supported this observation. It was theorized that this behavior, and the associated ineffectiveness of the slot jet to control boundary layer separation near the endwalls, could be reduced or eliminated by reorienting the shear layer vorticity as the end of the slot was approached. This led to the use of 2 types of non-linear slot shapes. In the first, when viewed from above, the slot sweeps away from the direction of flow as it approaches both endwalls. This configuration was called the rearward swept slot jet. In the second, the slot sweeps into the direction of flow as it approaches the endwalls, this configuration was called the forward swept slot jet.

3.4 Coflow Jet/Vortex Generators Theoretical Considerations

A primary goal in the diffusion enhancement aspect of flow control in this application was to energize fluid near the suction surface to overcome the adverse pressure gradient in that region. In the baseline configuration, this was done via mixing in the shear layer between the high speed secondary flow and the core flow. The shear layer strength, and therefore the mixing, is proportional to the velocity difference in the two streams. In an attempt to reduce the secondary air requirement and increase the overall mixing effect, vortex generators were placed on the suction surface just upstream of the slot jet. Various types and sizes of vortex generators were investigated. The objective was to optimize mixing and minimize loss due to the presence of the vortex generators.

It was postulated that increased streamwise vorticity would enhance the mixing between the main and secondary streams resulting in a persistent momentum exchange that will significantly delay separation. In order to impart this behavior, pairs of counter-rotating streamwise vortices were introduced via flat plate vortex generators placed on the upper surface of the flow control module plate as shown in Figure 10. The configuration generated vortex pairs for which their induced motion was toward the surface and the planar jet.

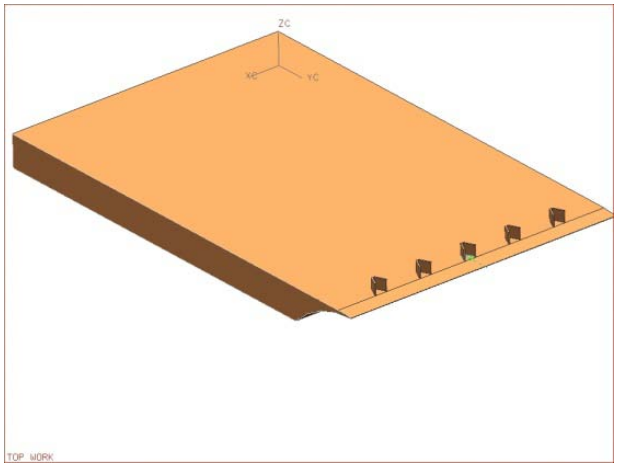

Figure 10: Vortex generators on the upper module plate

The desired circulation strength, Γ, and spacing, d, for the vortex pair was determined by taking a simplified approach to the flowfield. The streamwise velocity distribution was approximated as linearly varying from velocity V1 at the throat to V2. A relationship between streamwise position and time could then be obtained. An approximation of the circulation generated by a NACA 0012 vortex generator was used to relate the VG geometry to circulation strength. It was also assumed that the streamwise vortex pair advects with the background flow field. A functional relationship in the form of an inequality was generated relating the geometric parameters of the vortex generator with the diffusion characteristics of the passage:

$$\frac{F(AR, d/C)G(\alpha, h/\delta)}{H(DF)} \leq 1 \tag{1}$$

$$F(AR, d/C) = \left(\frac{AR + k_2}{k_1}\right)\left(\frac{d}{C}\right) \tag{2}$$

$$G\left(\alpha, \frac{h}{\delta}\right) = \left(\frac{1}{\alpha}\right)\left(\frac{1}{tanh[k_3(h/\delta)]}\right) \tag{3}$$

$$H(DF) = -\frac{4}{\pi^2} ln \frac{(1 - DF)}{DF} \tag{4}$$

where

$$k_1 = 1.61;\ k_2 = 0.48;\ k_3 = 1.41;\ k_4 = 1.00; AR = \frac{8}{\pi}\frac{h}{c};\ DF = 1 - \frac{V_2}{V_1}$$

where C is the surface arc length; c is the VG chord length; AR is the VG aspect ratio; h is the VG height; δ is the boundary layer height at the VG leading edge; α is the angle of attack; d is the distance between VG trailing edges (see Figure 11); V1 is the passage throat velocity; V2 is the passage exit velocity; and DF is a simplified diffusion factor as defined above.

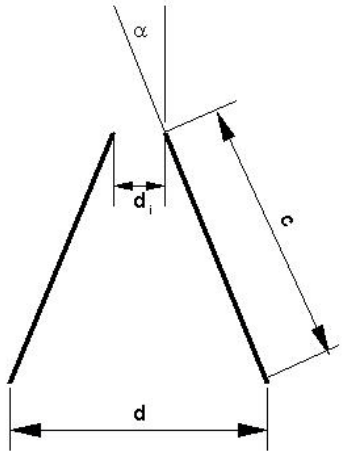

Figure 11: Counter-rotating vortex generator geometry definition

The function H is dependent only upon flow field kinematics (the diffusion factor). Both functions F and G are dependent on geometric characteristics along with the boundary layer thickness. A family of characteristic curves of FG/H were produced by fixing the function G through a choice of α and h/δ and the diffusion factor of 0.7 for the passage under consideration. Two geometric constraints were applied due to physical limitations of using these vortex generators. The first was due to the constraint of generating two counter-rotating vortices a distance d apart using vortex generators at an angle of attack α. Figure 11 shows a top-down view of the vortex generators with relevant dimensions. The second geometric constraint was derived from a heuristic argument that the distance, d, between the vortex pair should be less than the height of the vortex generator. This was applied so that the vortex image does not dominate initially and cause the vortex pair to migrate apart. A geometric configuration was chosen that maximizes the circulation and yet is acceptable according to the two geometric constraints. The boundary layer thickness for the wind tunnel at the throat was approximated from a CFD calculation at 0.254 mm. Using the surface arc length of the passage, C, of 31 mm gives the following VG geometric parameters: h = 3.81mm; d = 3.765mm; c = 3.962mm; α = 25°, d_i = 0.3765mm. Figure 10 shows the flow control

module upper plate obtained by using these geometric parameters at a spacing of 4.5 d between vortex generator pairs. The spacing between pairs of vortices was chosen based on guidelines outlined in [10].

3.5 Flow Control Using Discrete Jets

In an additional attempt to impart streamwise vorticity to increase diffusion capability of the stator passage, discrete jets were added to the suction surface of the stator airfoil. In this case, the previous slot jet injection device was replaced with a distributed array of discrete round holes. It was hypothesized that this change might provide equivalent diffuser performance at reduced control massflow. Though the spanwise coverage would be reduced by using discrete holes, greater mixing with the core flow would be expected, and the additional streamwise vorticity generated by the discrete jets could be advantageous.

Three rows of holes each were distributed on the suction surface of the passage. So-called “vortex generator jets” are reported in the literature with various angular orientations relative to the flow direction and the surface. In the current study, the holes were oriented in the streamwise direction at an 18-degree angle to the surface. The first row was placed at approximately the same location as the previous slot jet. The second row was placed at mid-passage, and the third was near the trailing edge.

4.0 RESULTS AND DISCUSSION

4.1 Co-flow Inset Jet

A preliminary CFD analysis was performed varying the momentum coefficient to determine its effect on the core flow. Figure 12 shows the baseline cascade and Figure 13 shows the flow control cascade with a momentum coefficient of 0.197, both with inlet conditions of M=0.7 and an inlet flow angle of 68 degrees with a desired exit flow angle of 0 degrees.

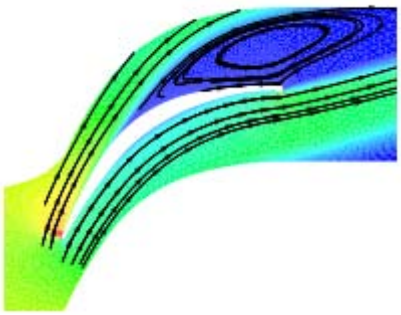

Figure 12: Non-controlled High Diffusion Blade

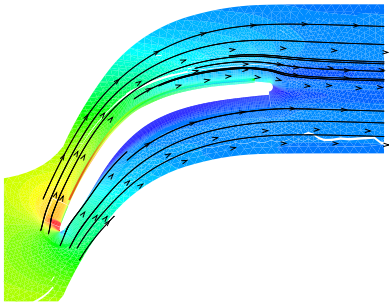

Figure 13: Controlled High Diffusion Blade

Figure 14 shows circulation, exit flow angle and diffusion factor versus momentum coefficient for the uncontrolled blade and two simulations of the controlled blade. As you can see from the figure, the slope of the circulation line is positive, i.e. it increases with increasing momentum coefficient. Therefore, blade loading is increased with increasing momentum coefficient.

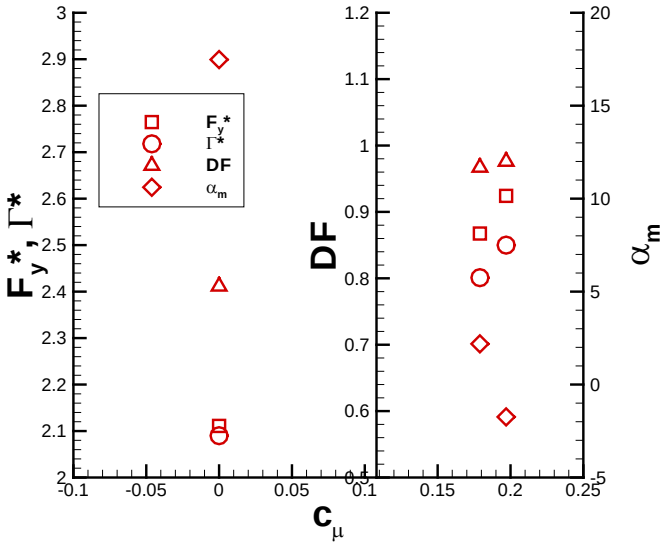

Figure 14: Non-dimensional Loading, Circulation, Diffusion Factor and Exit Flow Angle versus Momentum Coefficient

An availability analysis was performed to compare the net loss between the non-controlled and controlled blade. The non-dimensional availability for the blade is defined as,

$$\dot{\Psi}^* = -\frac{\left(\Delta s_c + f\Delta s_j\right)}{C_{p,c}} \tag{5}$$

where s is entropy; f is the flow fraction between the secondary flow and cp is the coefficient of specific heat at constant pressure. The subscripts c and j denote the core stream and secondary flow stream respectively. The mass averaged value was used for calculating the entropy in the CFD simulations. Figure 15 shows this parameter normalized by the non-controlled power. The controlled blade is shown with two different momentum coefficients. In the figure, the controlled blade attains over a 50% reduction in the amount availability (for a stator with no work input this amounts to irreversibility) greater than the non-controlled case. Therefore the process associated with the controlled blade produces less loss than the uncontrolled even when accounting for the secondary flow stream. It is important to recognize that this analysis does not include any losses that would be associated with the internal flow passages of the controlled blade.

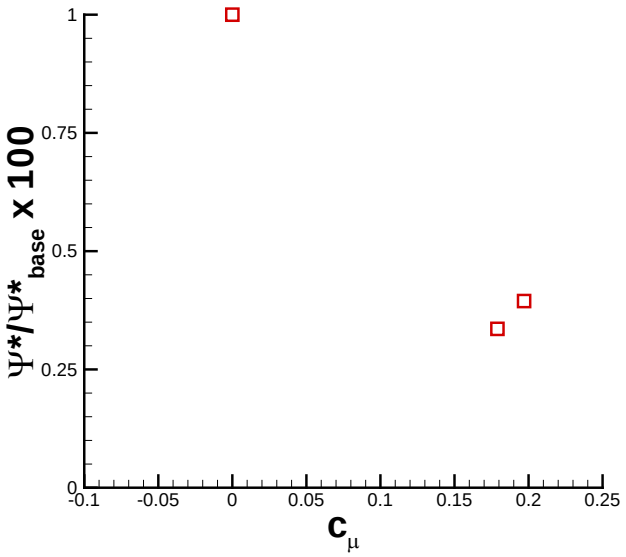

Figure 15: Availability versus Momentum Coefficient

A simple 1D power analysis was conducted to determine how this flow control technique would affect a single stage compression system with a pressure ratio of 4.0 and an adiabatic rotor efficiency of 0.90. An adiabatic efficiency of 0.72 was assigned to the secondary flow system to account for internal losses and held fixed for the analysis. It was determined form this analysis that a high momentum coefficient does not necessarily translate into a large penalty on compression system efficiency. Interestingly, either a high or low momentum coefficient achieving the same level of

diffusion requires a similar power input of the secondary stream. This means that the momentum coefficient for a given level of diffusion that achieves the lowest loss in the secondary flow delivery system is crucial when considering

While numerical modeling showed tremendous potential and experimental demonstration for external flow has shown promise [11], experimental demonstration in a cascade revealed the crucial role the airfoil-internal flow circuit plays in achieving the required boundary conditions to the core flow. The secondary flow system was found to be inadequate to provide the necessary inlet and outlet conditions at the blowing and suction slots. The experimental setup is shown in Figure 16 and Figure 17. Figure 16 shows the cascade as it was installed in the Virginia Tech blow down linear cascade facility. Each of the 4 blades contain the co-flow inset jet flow control device.

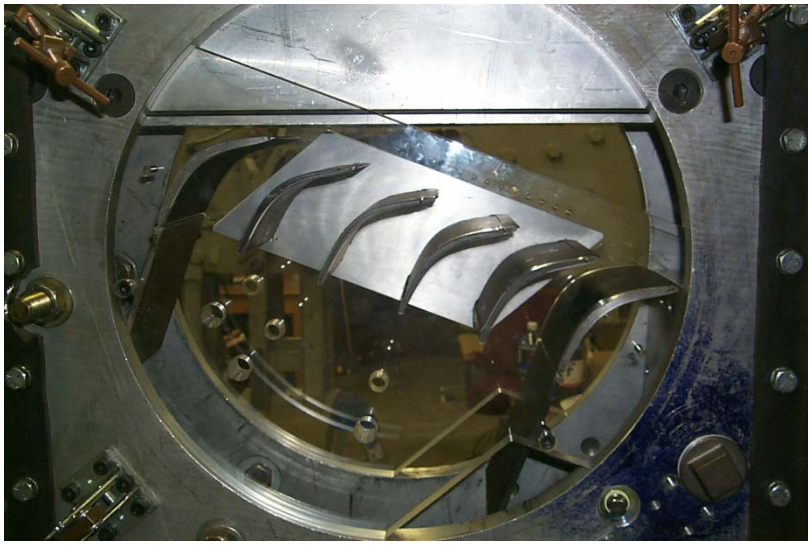

Figure 16: Cascade experimental setup shown in the Virginia Tech blow down cascade facility

Figure 17 illustrates how the PIV data was obtained. The PIV images were obtained in multiple segments. Two of the segments, labeled A and C in the figure, are shown.

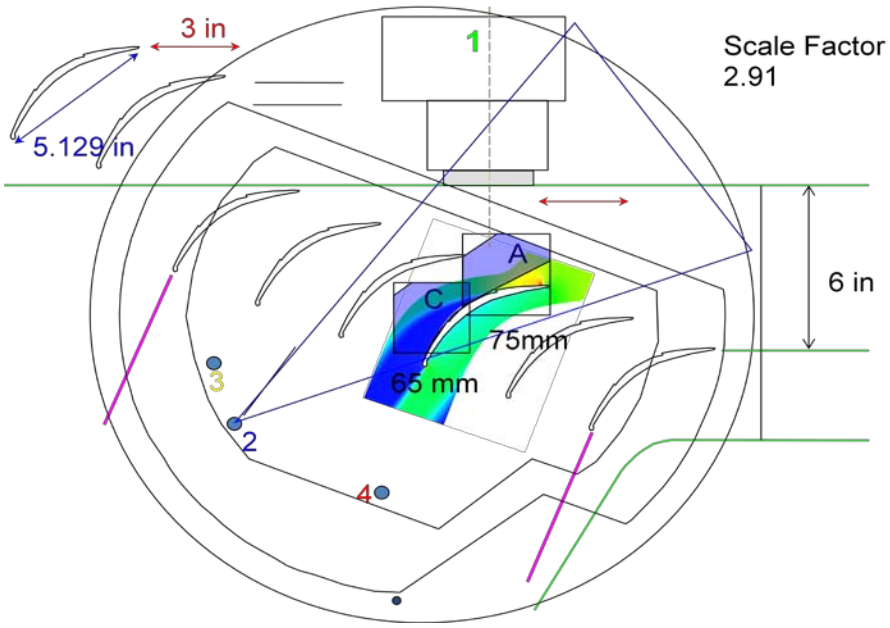

Figure 17: Experimental schematic showing PIV data acquisition fields

The controllable parameter obtained from a simple 2D control volume analysis is the momentum coefficient, c_μ, defined as:

$$C_\mu = \frac{\rho_j V_j^2 h}{\rho_1 V_{x1}^2 S} = \frac{\dot{m}_j V_j}{\dot{m}_c V_{x1}} \tag{6}$$

The subscript 1 denotes inlet conditions to the cascade section; j denotes the secondary flow jet; x is the axial Cartesian coordinate direction; h is the height of the injection slot for the secondary flow jet; S is the cascade pitch; V is velocity; ρ is density. The momentum coefficient defined here is simply the ratio of secondary flow momentum flux into the control volume to core flow axial momentum flux.

Because of the difficulties encountered with the secondary flow system, the cascade was run at a Mach number of 0.3 to achieve the equivalent momentum coefficient that would have been obtained at the design 0.8 Mach condition. Figure 18 shows PIV results obtained at that operating condition. Figure 18 a) shows the flow field in segment C from Figure 18 with the flow control off. The blue area indicates low velocity regions and the vectors indicate reversed flow indicative of boundary layer separation. Figure 18 b) shows the same segment with the flow control on. The region of low velocity fluid occupies a considerably smaller area.

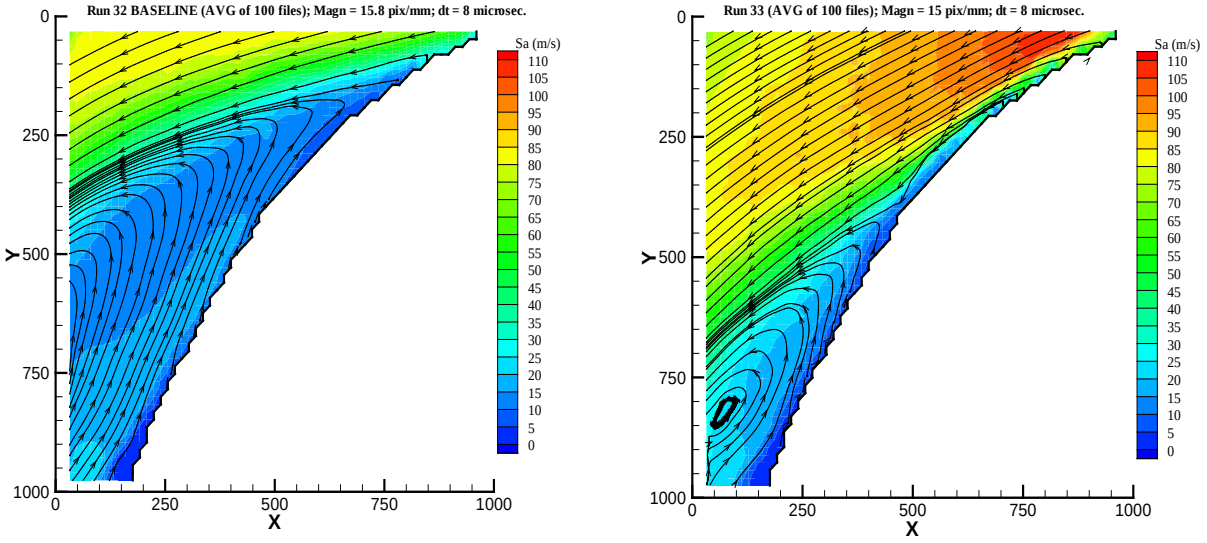

a) Uncontrolled flow condition **b) Control flow condition**

Figure 18: Cascade test results, flow control off and on

4.2 Co-flow Jet with Slot Jets

A thorough investigation of the performance of the co-flow concept with slot jets was performed. A concern with flow control of any type is the ability to fabricate the flow control device given typical machining limitations. The first area to investigate was the effect on the flow field of the thickness of the material between the core flow and the jet flow, i.e. the lip.

4.2.1 Lip Thickness Study

The influence of the separation distance between the core flow and jet flow due to the finite material thickness of the upper plate on the flow field was investigated [12]. Two material thicknesses were tested: 0.635 mm and 0.127 mm which are 125% and 25% of 2 the planar jet size respectively. The 0.127 mm thickness was achieved by honing the upper surface of the 0.635 mm plate at a 5 degree angle. Figure 19 shows the post processed DPIV average flowfield for a flow fraction of approximately 2% for both the 125% and 25% cases. The thinner lip thickness case (25%) shown in Figure 19 (b) indicates a much smaller separation region (blue region on the convex surface) than the thicker lip thickness case (125%).

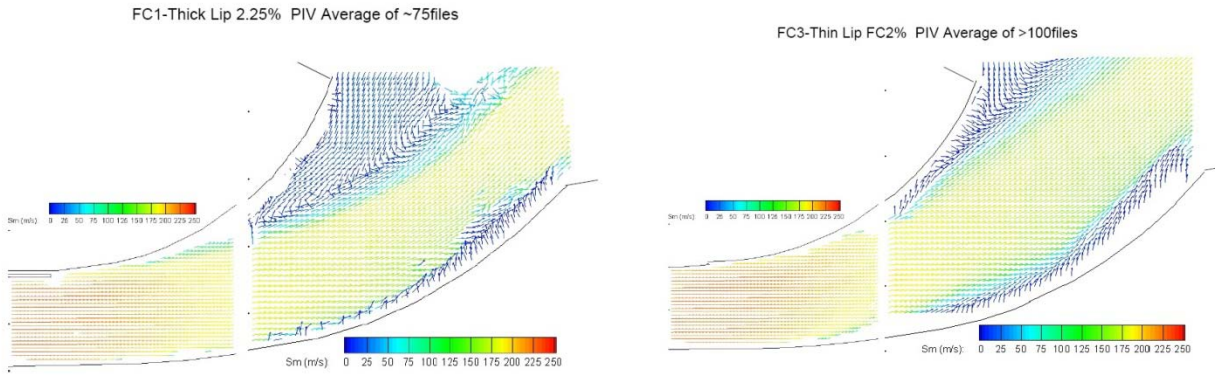

(a) Composite image of 125% primary to secondary separation distance and 2.25% flow control

(b) Composite image of 25% primary to secondary separation distance and 2.00% flow control

Figure 19: Effect of Core and Jet Separation on Diffusion Effectiveness

To further illustrate the impact of the thick vs. thin lip thickness, the pressure recovery factor was plotted against fraction of secondary flow in Figure 20. Again, from Figure 19, larger regions of flow separation exist for the 125% thickness case. Consequently, the 25% lip thickness requires half the secondary flow requirement for the same static pressure rise coefficient versus the 125% case as seen in Figure 20. The conclusion from this study is that there is a strong sensitivity of this particular flow control device performance to manufacturing details. Manufacturing limitations must be considered when reducing a flow control concept to practice.

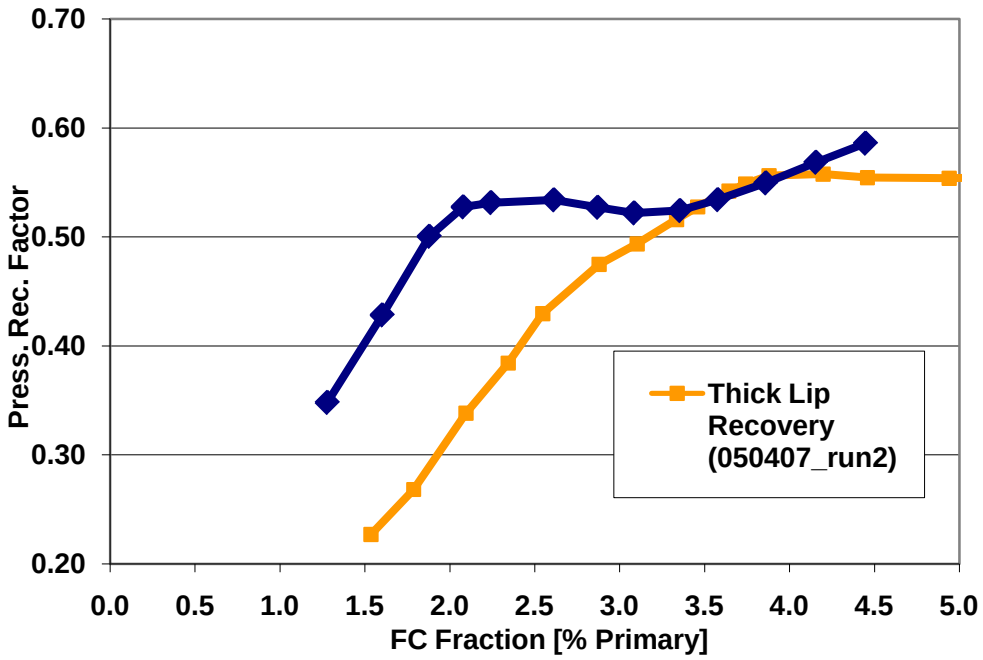

Figure 20: Effect of Core and Jet Separation on Static Pressure Recovery

4.2.2 Linear Slot Jet

The baseline for the series of slot jet configurations was the linear slot jet, shown installed in the flow control module in Figure 21. The slot jet height for these studies was fixed at 0.508 mm (0.020 in). A 5 degree chamfer exists on the end of the removable upper plate resulting in a 0.127 mm (0.005 in) lip thickness at the slot jet. This metal thickness is 25% of the jet height and was found to be a reasonable lip thickness size that results in an effective interaction between the slot jet and the core stream[12]. This metal thickness to jet height is maintained for all the modules outlined in this report. In this approach, high velocity flow is injected via a full span slot into the flow field near the suction surface parallel to the wall. Various momentum coefficients were investigated at a fixed throat (analogous to the stator leading edge) Mach number of 0.7. As the slot jet flow momentum is increased (i.e. increased flow fraction for a fixed slot height), exit total pressure traverse measurements showed a reduction in loss in the midspan region, but significant total pressure loss remained at the endwalls. The area averaged total pressure loss decreased from 16.4% to 9.8% for an overall total pressure increase of 6.6% at 4.5% flow fraction.

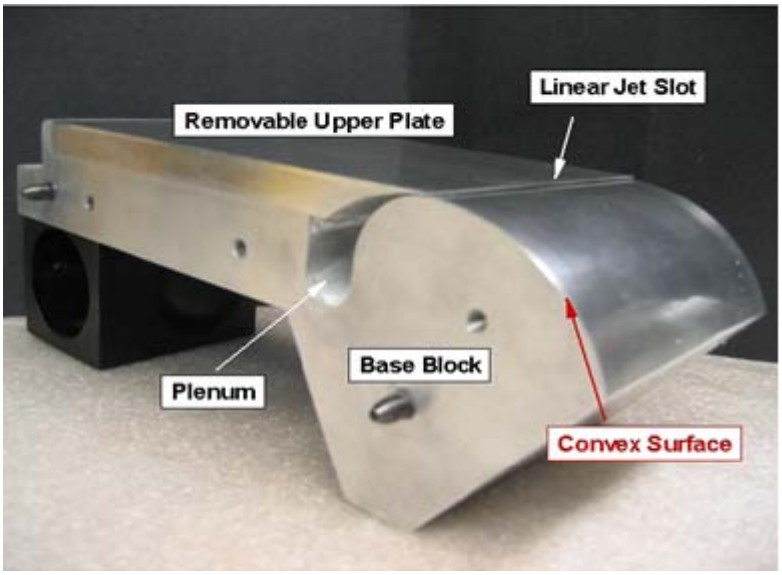

Figure 21: Linear slot jet configuration

Figure 22 through Figure 24 show the exit total pressure traverse for the 0, 3.0 and 4.5% secondary flow fraction levels. Both steady state measurements and the RMS value of consecutive measurements are shown as contours. The higher RMS values indicate where a wider variation occurred in the total pressure measurements. This indicates a local peak in unsteadiness. As the slot jet momentum is increased (i.e increased flow fraction for a fixed slot height), the exit total pressure traverse shows the loss reduction in the midspan region, but still a significant amount of total pressure loss at the endwalls. The area averaged total pressure loss decreases from 16.4% to 9.8% for an overall total pressure increase of 6.6% at 4.5% flow fraction. Note that the peak in unsteadiness occurs in the yellow and green areas for each of the conditions. This indicates the presence of a shear layer between the core flow and the jet flow.

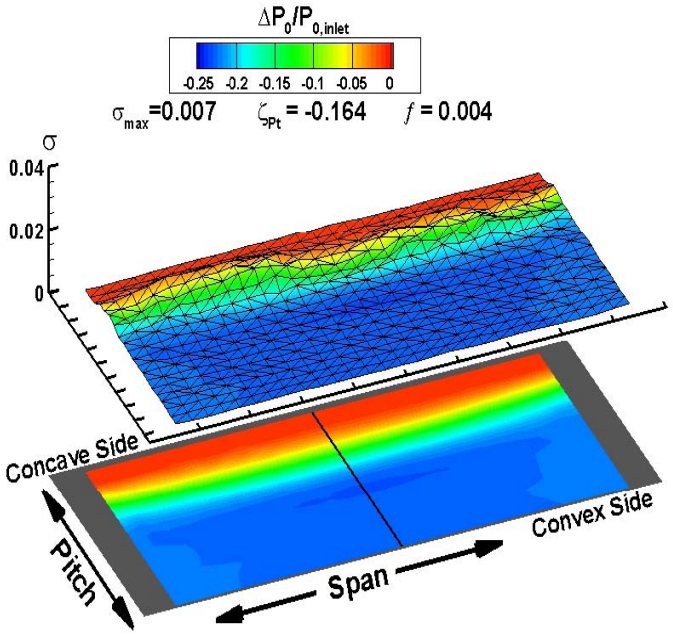

Figure 22: Test section steady (below) and unsteady RMS (above) total pressure for the linear slot jet with 0.4% flow fraction

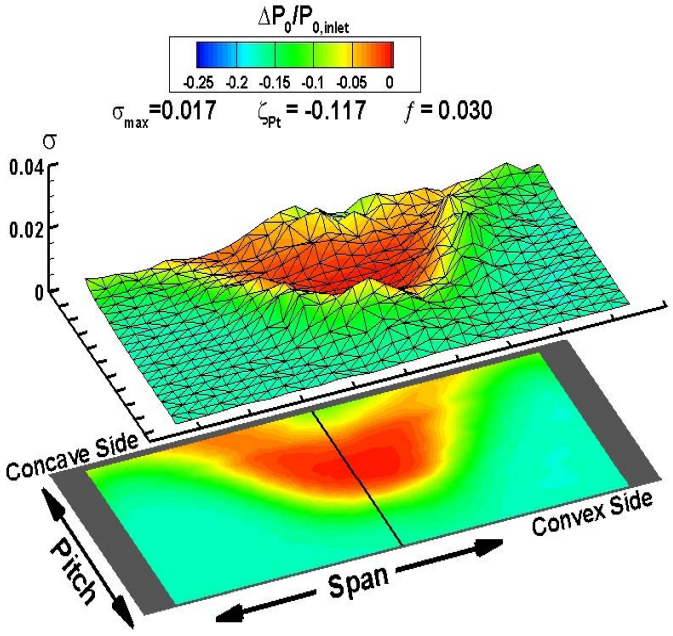

Figure 23: Test section steady (below) and unsteady RMS (above) total pressure for the linear slot jet with 3.0% Flow Fraction

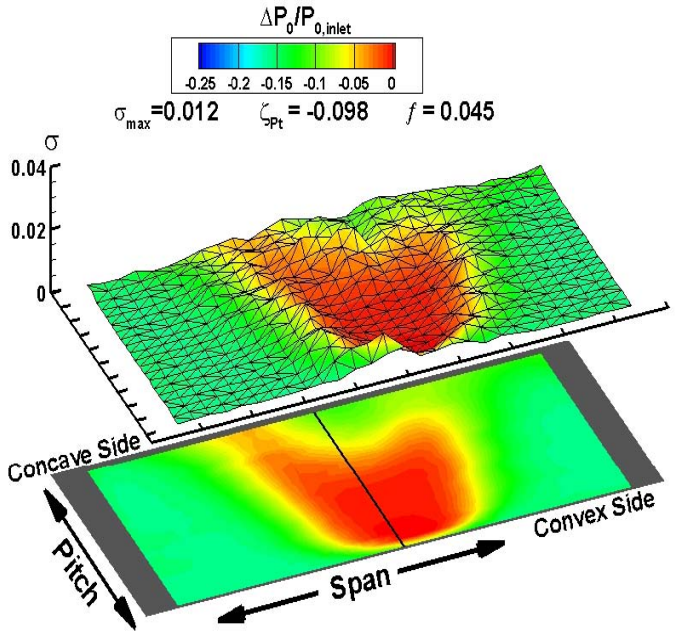

Figure 24: Test section steady (below) and unsteady RMS (above) total pressure for the linear slot jet with 4.5% flow fraction

4.2.3 Rearward Swept Slot Jet

Based the observed breakdown of the rolling vortex at the end of a finite slot jet [9], it was theorized that this behavior, and the associated ineffectiveness of the slot jet to control boundary layer separation near the endwalls, could be reduced or eliminated by reorienting the shear layer vorticity as the end of the slot was approached. This led to the use of 2 types of non-linear slot shapes. In the first, when viewed from above, the slot sweeps away from the direction of flow as it approaches both endwalls as shown in Figure 25.

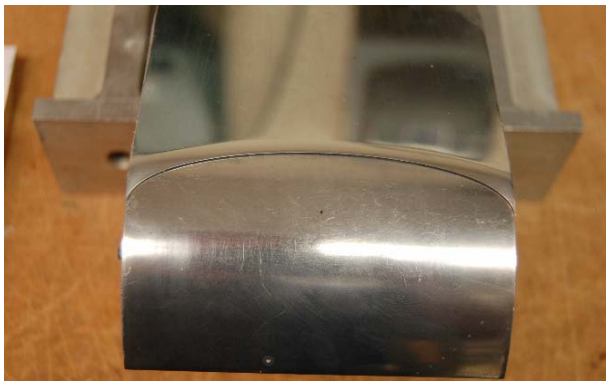

Figure 25: Rearward swept slot jet configuration

The upper plate of the slot module was modified to create a downstream sweeping motion at the endwalls. The endwall sweep extended 20 degrees over the convex surface and was created using an elliptical projection such that tangency was maintained at the endwalls. The ellipse was centered on the 20 degree radial line that passes through the convex surface center of radius. A Boolean subtraction was performed to create the final shape. The slot height was maintained at 0.508 mm (0.020 in) over the entire span and a 5 degree chamfer was added to the upper surface at the slot end to maintain a 0.127 mm (0.005 in) lip thickness as with the linear slot jet. The actual build of this module resulted in a uniform slot height at the desired 0.508 mm (0.020 in) as determined from feeler gauges.

Figure 26 through Figure 28 show the gauge total pressure exit traverses for this configuration at 0, 3.0 and 4.25% flow fraction. Endwall effects are still pronounced throughout the entire flow range recorded. A more narrow distribution of exit total pressure is apparent when comparing these results with the linear slot jet. The levels of loss are comparable to the linear slot jet, with the linear slot jet showing slightly better performance. This configuration has lower levels of unsteadiness than the linear slot jet configuration.

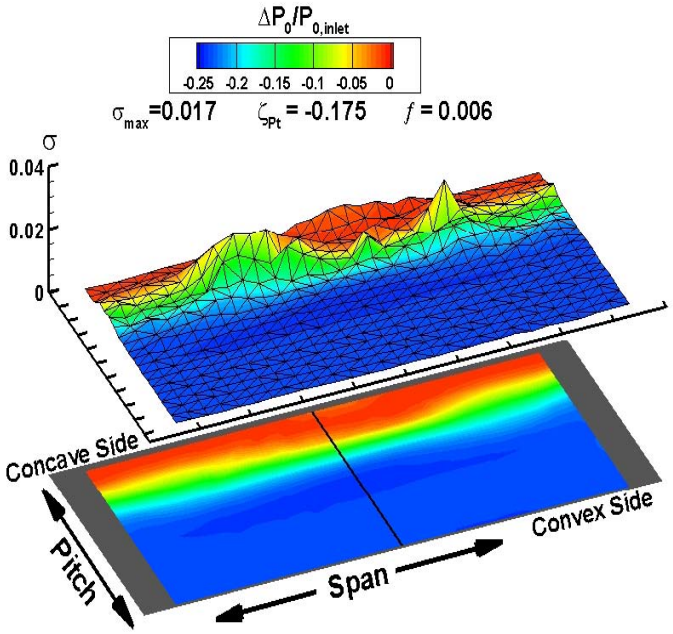

Figure 26: Test section steady (below) and unsteady RMS (above) total pressure for the rearward swept slot jet with 0% flow fraction

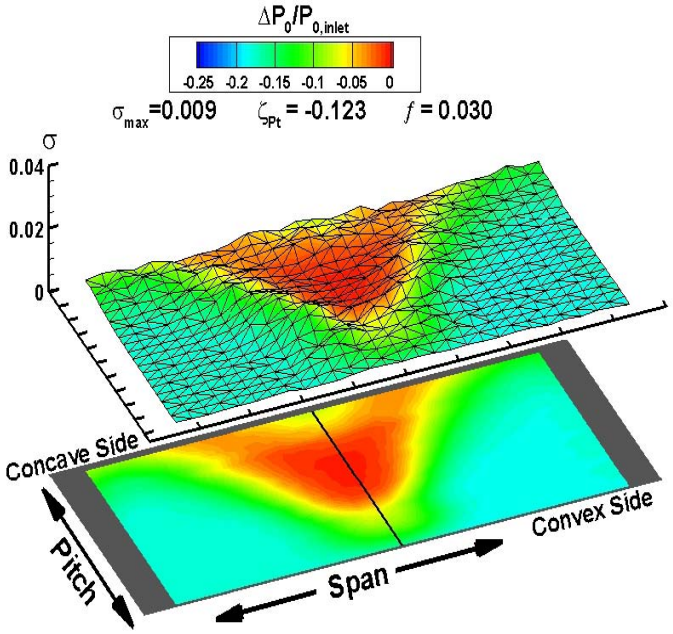

Figure 27: Test section steady (below) and unsteady RMS (above) total pressure for the rearward swept slot jet with 3.0% flow fraction

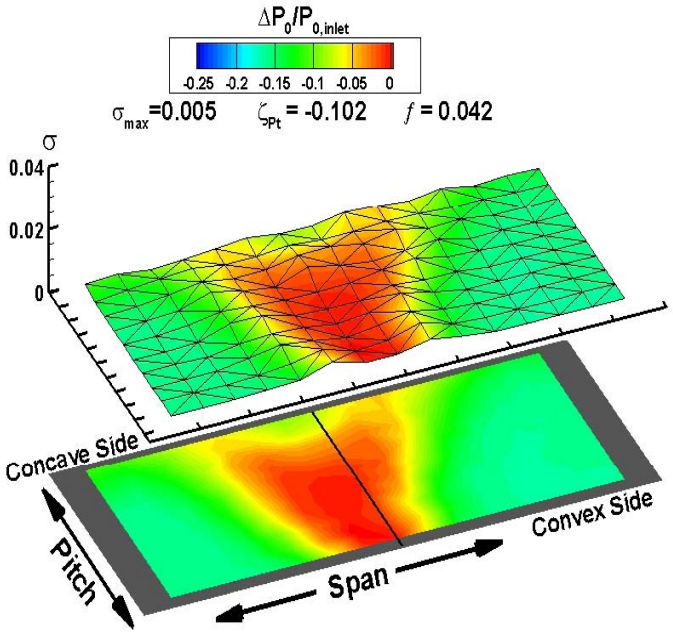

Figure 28: Test section steady (below) and unsteady RMS (above) total pressure for the rearward swept slot jet with 4.25% flow fraction

4.2.4 Forward Swept Slot Jet

In this configuration the slot was shaped so that, when looking from above, the slot sweeps into the direction of flow as the endwalls are approached. This was accomplished by sweeping the upper plate 20 degrees over the convex surface and projecting an ellipse onto the surface such that tangency was maintained at the endwalls. The elliptical projection was created by centering an ellipse on the zero degree radial line that passes through the throat of the tunnel and intersects the convex surface center of radius. A Boolean subtraction with the upper plate was performed to create the shape as shown in Figure 29 [13]. The slot height was maintained at 0.508 mm (0.020 in) over the entire span and a 5 degree upstream chamfer was added to the upper surface at the slot end to maintain a 0.127 mm (0.005 in) lip thickness, the same as with the linear slot jet. The actual build of this module resulted in a uniform slot height of approximately 0.508 mm (0.020 in) as determined from feeler gauges.

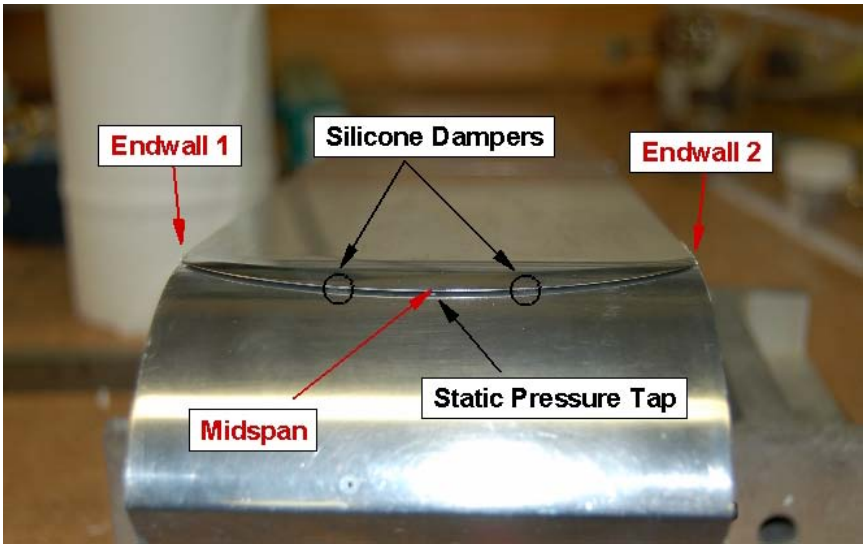

Figure 29: Forward swept slot jet configuration

It was not possible to achieve a choked slot condition during the experiment due to a plate resonance that occurred just before a choked condition. This resonance condition was not surprising due to the relatively delicate nature of the design with an approximate 0.508 mm (0.020 in) thickness extending outward over 20 degrees of the convex surface. A modification of the design was performed in order to damp this resonance condition. The modification was to place a 0.584 mm (0.023 in) thick strip of self-adhering silicone sheeting approximately 3.175 mm (0.125 in) wide under the extended portion of the upper plate at 33% and 66% span. This effectively discretized the slot jet into three slot jets separated by 3.175 mm (0.125 in). The silicone sheeting thickness was larger than the intended slot jet height resulting in assembled spanwise

slot jet height variation. Feeler gauge measurements revealed a slot jet height of 0.5334 mm (0.021 in) at the endwalls and a larger 0.635 mm (0.025 in) at the midspan. This was an unavoidable consequence, but necessary to achieve a choked slot jet condition.

Figure 30 through Figure 33 show the gauge total pressure exit traverses as described in the previous section. The first two flow conditions (0% and 3.15%) show very similar behavior to the linear slot jot presented in the previous section in terms of loss level and poor endwall performance. One notable difference with this configuration is the increased level of low frequency unsteadiness as seen in the standard deviation of the data set. A very interesting transition occurs between the 3.15% and 3.5% flow fraction. What could be described best as an "inversion" of the exit total pressure field occurs, resulting in the endwall flowfield improving and the midspan region degrading in terms of total pressure (please note the contour scale change between Figure 31 and Figure 32 in order to resolve the exit flow features better). The standard deviation increases over the entire exit plane with max levels slightly lower than the 3.15% case. As the flow fraction level is increased, the unsteadiness reduces dramatically with 1/4 the value of max standard deviation at 4.0% flow fraction and overall area averaged total pressure loss reaching a level of 9.8% at 4.5% flow fraction.

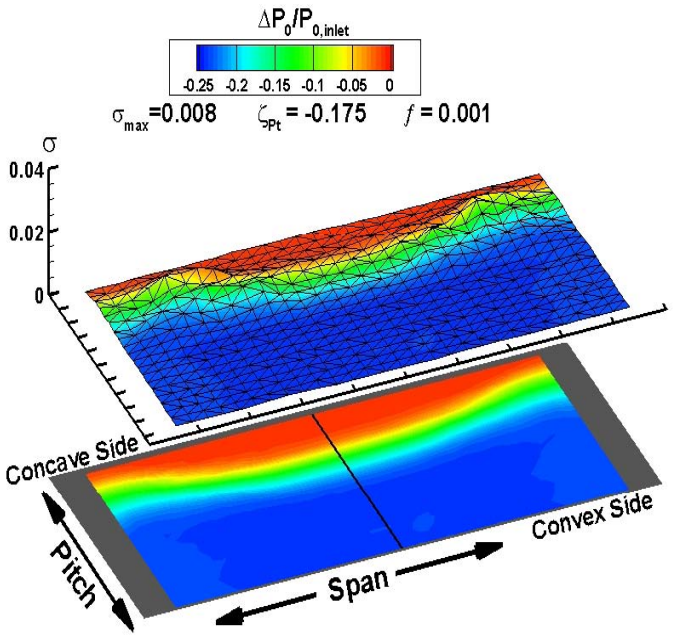

Figure 30: Test section steady (below) and unsteady RMS (above) total pressure for the forward swept slot jet with 0% flow fraction

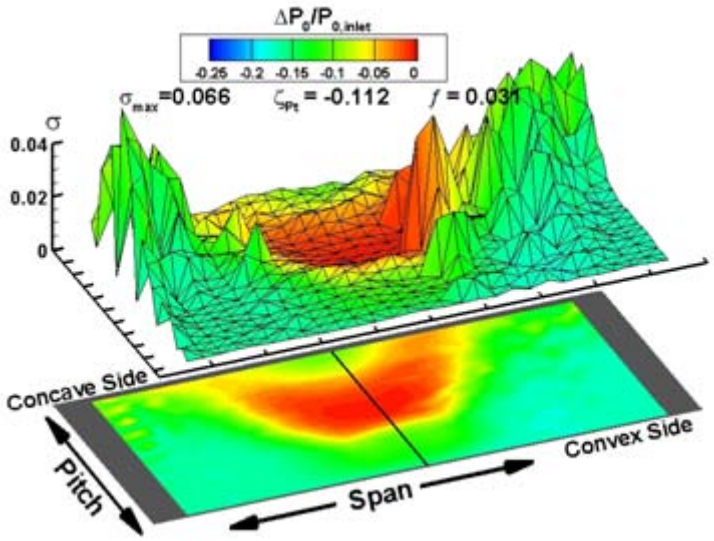

Figure 31: Test section steady (below) and unsteady RMS (above) total pressure for the forward swept slot jet with 3.1% flow fraction

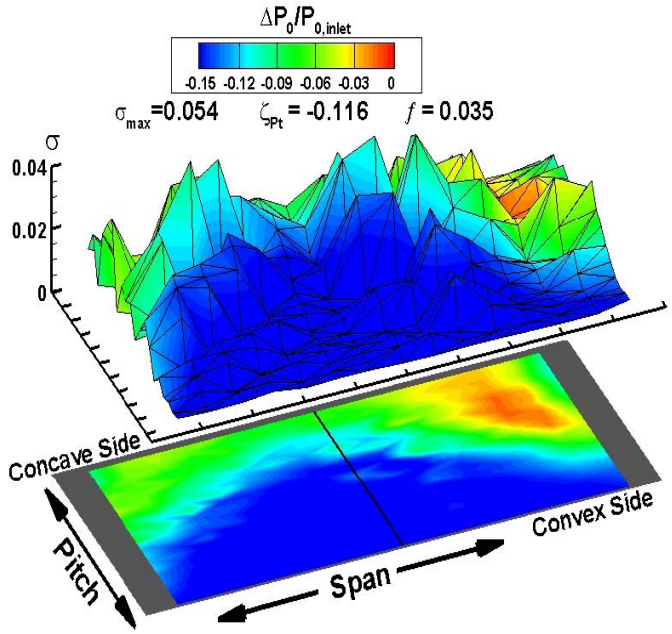

Figure 32: Test section steady (below) and unsteady RMS (above) total pressure for the forward swept slot jet with 3.5% flow fraction

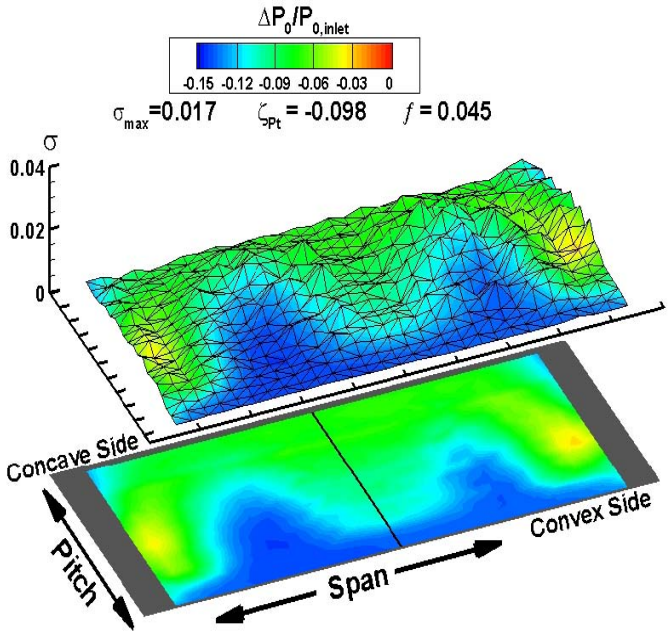

Figure 33: Test section steady (below) and unsteady RMS (above) total pressure for the forward swept slot jet with 4.5% flow fraction

4.3 Co-flow Jet with Vortex Generators

In order to enhance and extend the mixing between the near wall flow and the core flow, vortex generators were employed on the upper surface of the linear slot jet as shown in Figure 34 [13]. A spanwise arrangement of flat-plate vortex generator fins was used such that repeating pairs of counter-rotating streamwise vortices would be generated above the core flow surface of the flow control module just upstream of the linear slot jet and its lead-in chamfer. Care must be taken when using counter-rotating vortices due to the induced motion of the vortices on one another [14], [15].. The counter-rotating vortex generator arrangement was designed based on the detailed methodology described in [4] with the intent that the induced motion of the vortices would be toward the slot jet and convex surface. The selected design utilized rectangular fins normal to the surface and inclined at 25^{o} to the flow direction, with chord of 3.96 mm (0.156 in). The distance between trailing edges of paired fins, d, was 3.77 mm (0.148 in), while a spacing of 4.5d between neighboring pairs is used.

Secondary flow fractions from 0 to 6% of the core flow were investigated. Large improvement was seen at midspan but significant low momentum fluid generally remained at the endwalls. A portion of the flow control range between 4.5% and 5.9%

was unstable. As the flow control fraction was increased to 5.9%, however, the bulk flow re-stabilized to a symmetric pattern with well-behaved endwalls.

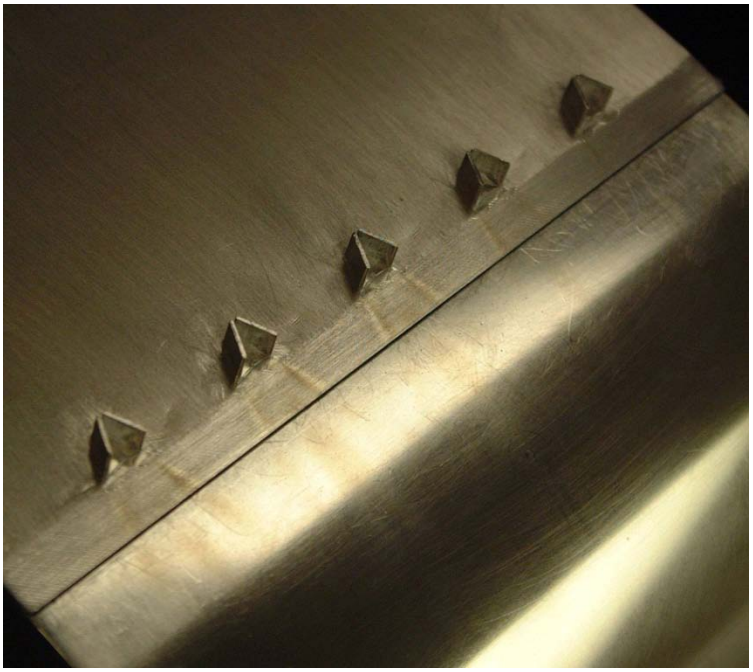

Figure 34: Vortex generators applied to the upper plate on the linear slot jet configuration

Figures 6 through 8 show the exit surveys for this configuration, operated at flow control fractions of 0.0, 3.0 and 5.9%. At 0% flow control, there are several peaks in the standard deviation distribution suggesting that these regions have increased low-frequency unsteadiness. For increasing flow control, the exit distribution again becomes more three-dimensional, but the region of negligible loss does not extend as far towards the convex surface as the LSJ. At and above 4.0% flow control, there are local pockets of lower total pressure fluid initially appearing near the convex surface just on either side of the midspan line. These may indicate the location of persisting vortex cores from the tall VGs. A portion of the flow control range between the 4.5% and 5.9% cases was unstable, leading to overall flow unsteadiness, some asymmetry and marginal stability. As the flow control fraction was increased towards 5.9%, however, the bulk flow re-stabilized to a symmetric pattern as shown in **Error! Reference source not found.**.

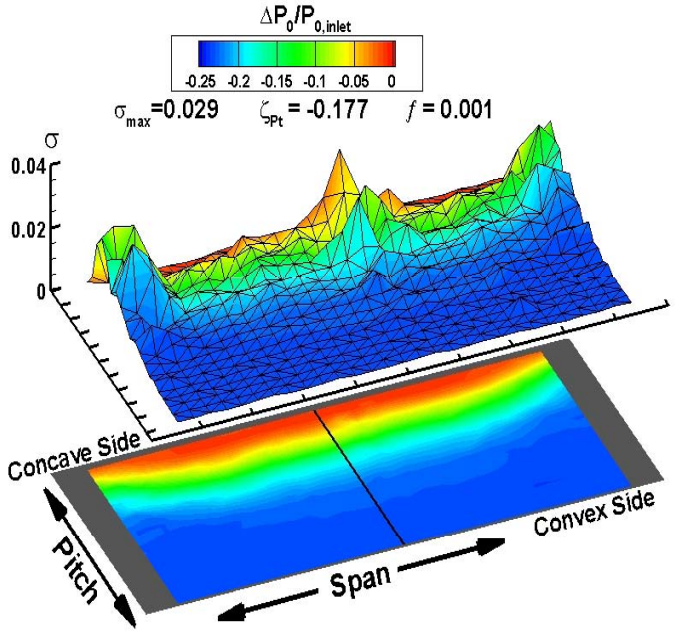

Figure 35: Test section steady (below) and unsteady RMS (above) total pressure for the linear slot jet with vortex generators at 0% flow fraction

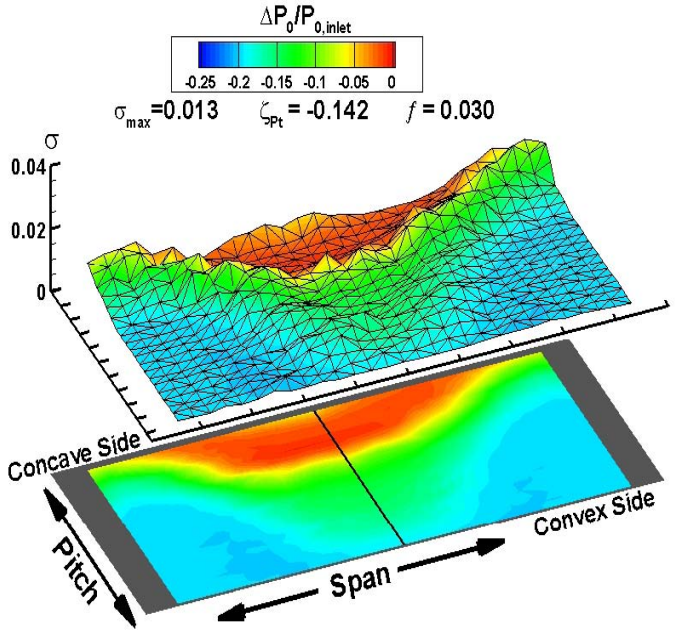

Figure 36: Test section steady (below) and unsteady RMS (above) total pressure for the linear slot jet with vortex generators at 3.0% flow fraction

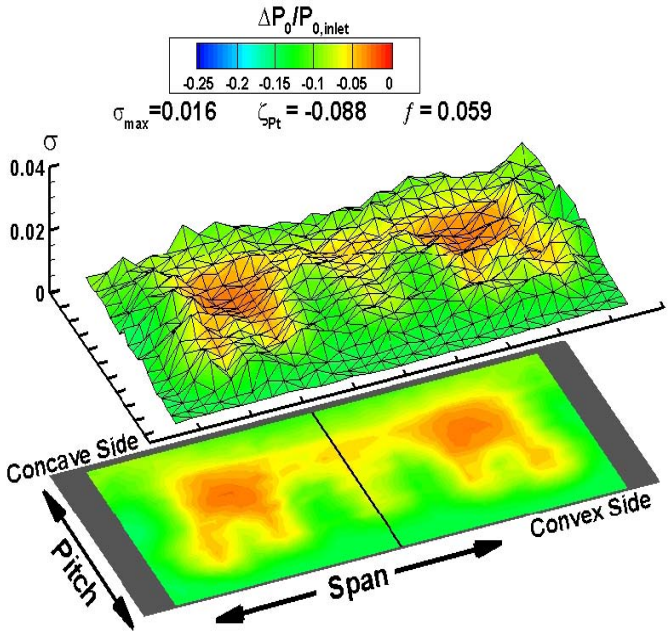

Figure 37: Test section steady (below) and unsteady RMS (above) total pressure for the linear slot jet with vortex generators at 5.9% flow fraction

4.4 Discrete Jets

Three identical rows of 21 holes each were distributed on the suction surface of the passage, with the total cross-sectional area of the holes being equivalent to that of the slot jet. The hole diameter (1.02mm) was also nearly identical to the hydraulic diameter of the slot. The holes were streamwise at an 18-degree angle to the surface, and the hole pitch-to-diameter ratio was 4.75. The first row was placed at approximately the same location (10deg) as the previous slot jet, that is, near the entrance to the curved diffuser. The second row was placed at mid-passage (35deg), and the third was near the trailing edge (60deg). Independent plenums fed each of the three rows.

Two different versions of this configuration, shown in Figure 38, were built and tested. The first has five vortex generator jets in the diffuser throat, upstream of the 3 rows of holes. The vortex generator jets are inclined at 45 degrees to the surface with zero skew angle to each produce a pair of counter-rotating vortices. The second version has solid vortex generators extending from the surface one boundary layer thickness, each with a small hole in their trailing edge to permit an active jet of air to be emitted. It was hypothesized that the active jet might cause streamwise stretching of the vortices, thereby extending their effect further downstream. In both cases the locations of the

vortex generating features are the same as previously used for vortex generators combined with a slot jet.

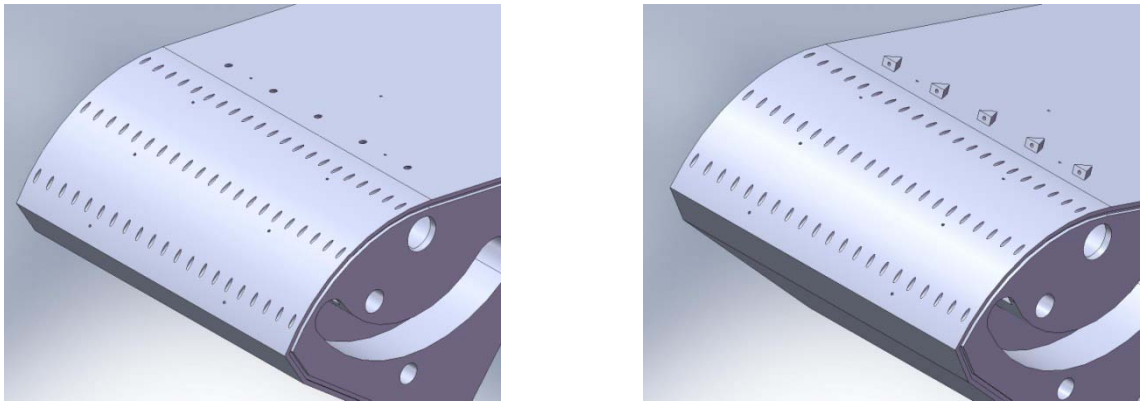

(a) Vortex generator jets **(b) Active vortex generators**

Figure 38: Distributed discrete hole flow control modules

Three different modules built by a conventional stereolithography technique were tested. Two of the modules are those depicted in Figure 38. For the third module, which was a variation of the innovative and effective forward swept slot jet, a boundary layer bleed slot was included just upstream of the module throat. The goal was to completely remove the incoming boundary layer on the suction side, thereby increasing the similarity of the diffuser passage to a compressor stator passage. However, further testing of this configuration was not accomplished before program termination.

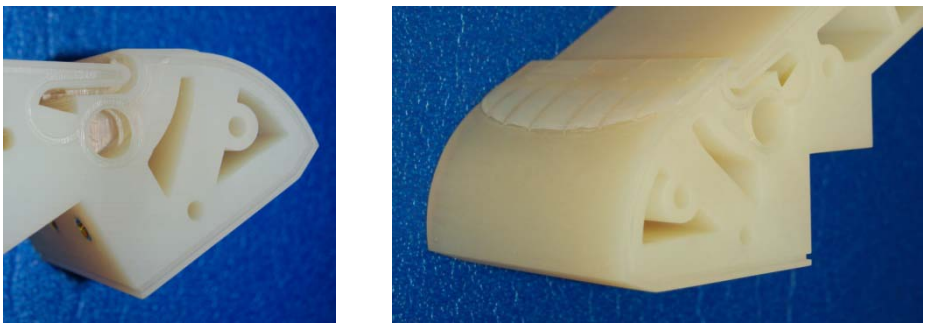

Figure 39: SLA flow control module with boundary layer bleed and forward swept slot jet

A new clean seed system under development in conjunction with the flow control research activities was used to capture some instantaneous flow visualization images for the distributed discrete jet flow control configuration (ref. Figure 38 a). Two such images, taken at midspan, are provided in Figure 40. In both images the throat flow is

at Mach 0.7 and the vortex generator jets, emanating from the far left of the convex surface, are choked. With only the vortex generator jets on in Figure 40a, the jet penetration and related turbulent structures are seen, but little flow turning is evident and a large separation remains. In Figure 40b, the first and second flow control hole rows are run at choked conditions. The resulting increase in vectoring and reduction of the separation are evident. However, turbulent structures are more pronounced on the concave surface, perhaps indicating incipient separation there.

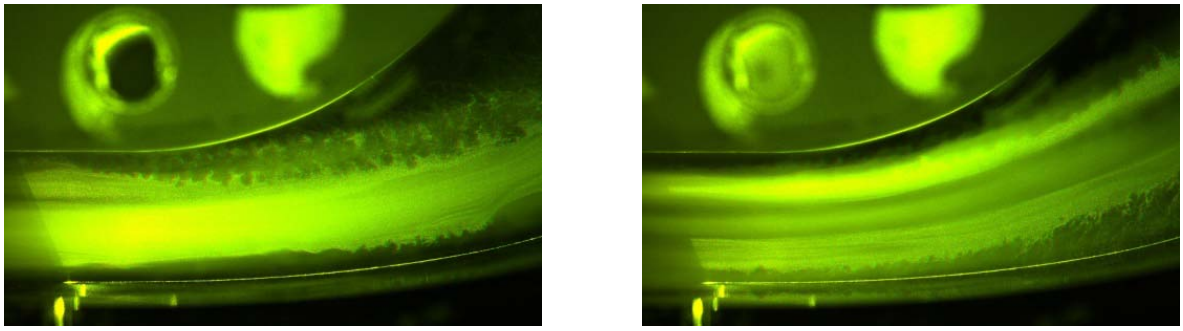

(a) Vortex generator jets operating

(b) Vortex generator jets operating plus rows 1 and 2 of the discrete flow control holes operated at choked conditions

Figure 40: Instantaneous flow visualization images

Total pressure surveys at the diffuser exit were used to characterize overall performance of the various flow control configurations. Figure 41 shows the performance of the various discrete hole test cases, both with and without vortex generators, in comparison to the previous linear slot jet case. It is evident that all the discrete hole configurations without VGs were more effective than the linear slot jet at reducing losses for low flow control inputs. However, at higher inputs the linear slot jet provided greater loss reduction benefits. It appears that the discrete hole flow control was unable to sufficiently offset the higher pressure losses of the vortex generators, which is in contrast to previous findings for the combination of the linear slot jet with vortex generators. For compactness the test cases with vortex generator jets and vortex generators in active mode are excluded, since these showed no performance benefit in the present study.

Though not shown here, it is noteworthy that the baseline (no injection) losses *with* short VGs (less than the BL thickness) in the LSJ configuration were lower than *without* VGs or FC in the discrete hole configuration. This suggests that small VGs, properly arranged, can indeed reduce losses for highly loaded diffusers.

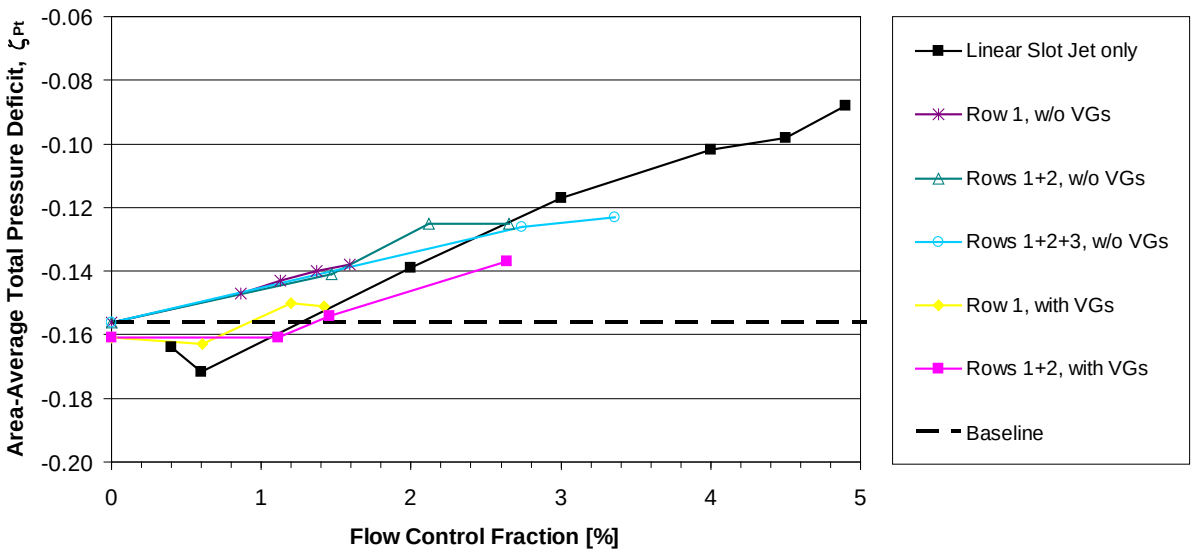

Figure 41: Effect of various flow control configurations on diffuser total pressure losses

4.5 Summary of Flow Control Activities for High Loading

Various configurations of momentum injection are used to increase the diffusion level of a curved, diffusing wind tunnel which simulates an extremely highly loaded axial compressor stator passage. The entrance Mach number to the passage is 0.7 with mass injection fractions ranging up to six percent. The throat aspect ratio (throat height to span ratio) is approximately 7:1 and the diffusing section of the passage has a radius of curvature of 5.08 cm for the convex surface. Several variations of multi-row discrete hole injection are compared to linear slot jet injection results. Traditional vortex generators, active vortex generators, and vortex generator jets were used to augment streamwise vorticity production, which was previously shown to benefit diffuser performance. Without streamwise vorticity augmentation, the discrete hole configuration was shown to be more effective than the linear slot jet for reducing diffuser total pressure losses at low injection rates. However, the linear slot jet showed greater loss reduction than discrete holes at high injection rates. The use of vortex generator jets, vortex generators or active vortex generators with the distributed discrete hole flow control configuration was not shown to be beneficial. While all of the flow control configurations tested to date have demonstrated substantial improvement in the diffuser midspan performance, effective control of the endwall flowfield remains a distinct challenge and will require further study.

The focus of activities thus far has been on maintaining an attached boundary layer on the convex surface of a curved diffuser that is undergoing an extremely aggressive adverse pressure gradient. In addition, the flow conditions investigated have been representative of those in a modern high performance compression system. The entrance (or stator leading edge) Mach number investigated was 0.7. In this flow regime, a significant degree of flow control authority is required to improve the condition of the boundary layer. Early in this work a system study was conducted to determine the cycle benefit of flow control applied to the compression system. Depending on which cycle parameters were held constant, thrust-to-weight and engine volume improvements were demonstrated. With this potential benefit in mind, several conceptual, analytical, and experimental activities have been pursued at the basic research level to support transition to 6.2 and beyond.

5.0 CONCLUSIONS

An investigation of the use of flow control to increase the loading capacity of stator blade row has been completed. The majority of the work focused on spanwise slot jets of varying configurations. A system study was performed which indicated that if sufficient loading increase could be achieved, then the gas turbine cycle would benefit even given the irreversabilities associated with the secondary flow system. The secondary flow system must be given close scrutiny for such applications in terms of its performance. While high efficiency of the secondary flow system may not be paramount, its ability to deliver and scavenge (as necessary) flow at the proper conditions will enable the flow control's positive effect on the flow field. Of the many configurations investigated, the consistent observation was that mixing between streams must be enhanced in order to gain sufficient benefit from the flow control device. Further, the key to achieving mixing was through the addition of streamwise vorticity. Finally, for all of the configurations investigated for this very highly loaded case, fairly large secondary flow fractions were required to make an impact on the flow. Generally up to 5 and 6 percent of the core fow.

6.0 PUBLICATIONS

The following publications were generated during the effort described in this report.

Bailie, S.T., Ng, W., Wicks, S., and Copenhaver, W.W., "Effects of Flow Control on Forced Response and Performance of a Transonic Compressor, "ASME Turbo Expo, GT-2002-30008, June 2002.

Bloch, G., Loellbach, J., and Hah, C., "A Numerical Investigation of the Interaction between Rotor Bow Waves and Upstream Wake Generators in a Transonic Compressor Stage," 4th ASME/JSME Joint Fluids Engineering Conference, July, 2003.

Car, D., Bailie, S. T., Baudendistal, C., Gebbie, D., Estevadeordal, J., "Fluidic Control Studies for Diffusion Enhancement in Axial Compression Systems", 44th AIAA Aerospace Sciences Meeting and Exhibit, Reno, NV, 2006, AIAA Paper No. 2006-0417.

Car, D., Kuprowicz, N.J., Estevadeordal, J., Zha, G., and Copenhaver, W.W., “Stator Diffusion Enhancement Using a Re-circulating Co-flowing Steady Jet,” ASME Transactions, GT2004-53086, June, 2004.

Copenhaver, W., Estevadeordal, J., Gogineni, S., Gorrell, S., and Goss, L., 2002, “DPIV study of near-stall wake-rotor interactions in a transonic compressor,” Exp. In Fluids, Exp Fluids (2002) 33: 899-908, december (special issue on PIV).

Copenhaver, W.W., Estevadeordal, J., Gogieni, S., Gorrell, S.E., and Goss, L., “DPIV study of Near-Stall Wake-Rotor Interactions in a Transonic Compressor, “4th International Symposium of Particle Image Velocimetry, April 2002, Accepted for publication in Experiments in Fluids Journal.

Estevadeordal, J. and Copenhaver, W.W., “Milli-DPIV studies of a boundary-layer based flow control system for a transonic cascade”, Abstract and presentation for the 55th APS/DFD Conference, Dallas, TX, 24-26 Nov 2002, Vol. 40, N. 10.

Estevadeordal J., Gorrell, S.E., and Copenhaver, W.W.,"PIV Study of Wake-Rotor Interactions in a Transonic Compressor at Various Operating Conditions," AIAA Journal of Propulsion and Power (Revision submitted April 06-)

Estevadeordal, J. and Goss, L.P., "An Investigation of Particle-Shadow Velocimetry (PSV) for Transonic-Flow Applications," AIAA 35th Fluid Dynamics Conference, Paper AIAA-2005-5009, June 6 - 9, 2005, Toronto, CANADA

Estevadeordal, J., Copenhaver, W.W., and Car, D., 2003 “Mili-DPIV Approaches for Studying Boundary-Layer Based Flow Control Systems,” Abstract and Presentation at the AIAA 28th Annual Dayton-Cincinnati Aerospace Science Symposium, March 4.

Estevadeordal, J., Gogineni, S., Goss, L., Copenhaver, W.W., and Gorrell, S.E., “Study of Wake Blade Interactions in a Transonic Compressor Using Flow Visualization and DPIV,” Journal of Fluids Engineering, Vol. 124, March 2002, pp. 166-175.

Estevadeordal, J., Gorrell, S., and Copenhaver, W., “PIV study of wake-rotor phenomena in a transonic compressor under various operating conditions,” AIAA J. of Propulsion and Power, Volume 23, Number 1, 2007, pp. 235-242.

Estevadeordal, J., Gorrell, S., Gebbie, D., Puterbaugh, S., “PIV Study of Blade-Row Interactions in a Transonic Compressor,” Proceedings of the 43th AIAA/ASME/SAE/ASEE Joint Propulsion Conference and Exhibit, AIAA-2007-5017, 2007.

Estevadeordal, J., Guillot, S., Ng, W., Koch, P., Car, D., Puterbaugh, S., 2004 “Benefits of suction-surface blowing in a transonic compressor stator vane” AIAA-2004-2207; AIAA 2nd Flow Control Meeting, ‘Gas Turbine Engine Flow Control’ , Portland OR, June 28-July 1, 2004.

Gebbie, D., Gorrell, S., and Estevadeordal, J., “Development and Application of an Improved PIV System for Turbomachinery Applications,” Abstract and Presentation for 59th Annual Meeting of the APS Division of Fluid Dynamics, Tampa, Florida, November 19–21, 2006.

Gebbie, D., Gorrell, S., and Estevadeordal, J., “PIV Study Of Stator Loading Effects On Vortex Shedding In Transonic Compressor,” Presentation at the 32st Annual AIAA Dayton-Cincinnati Aerospace Science Symposium, Dayton, Ohio, March 6, 2007.

Gogineni, S., Estevaderodal, J., Copenhaver, W.W., and Gorrell, S. “ Investigation of Wake-Shock Interaction in a Transonic Compressor using DPIV,”, Proceeding of the 25th International Airbreathing Engines Conference, ISOABE-2001-1196, Sept. 2001.

Gorrell, S. E., Car, D., Puterbaugh, S. L., Estevadeordal, J., and Okiishi, T., "An Investigation of Wake-Shock Interactions in a Transonic Compressor with DPIV and Time-Accurate CFD," Proceedings of GT2005, ASME Turbo Expo 2005: Power for Land, Sea and Air, June 6-9, 2005, Reno-Tahoe, Nevada, USA; Paper GT2005-69107. Accepted for publication in J. of Turbomachinery

Gorrell, S. E., Car, D., Puterbaugh, S. L., Estevadeordal, J., and Okiishi, T., “An Investigation of Wake-Shock Interactions in a Transonic Compressor with DPIV and Time-Accurate CFD,” J. of Turbomachinery, Vol. 128, Issue 4, 2006, p. 616.

Gorrell, S., Copenhaver, W., and Estevadeordal, J.; 2003 'DPIV Measurements of the flow field between a transonic rotor and an upstream stator', ISUAAAT 03, International Symposium on Unsteady Aerodynamics, Aeroacoustics & Aeroelasticity of Turbomachines, Sept 7-11, 2003 Duke University, Burham, NC.

Gorrell, S.E., Okiishi, T., and Copenhaver. W.W., “Stator-Rotor Interactions in a Transonic Compressor, Part 1 Effect of Blade Row Spacing on Performance,” Accepted for publication in the ASME Journal of Turbomachinery, ASME Turbo Expo, GT-2002-30494, June 2002.

Gorrell, S.E., Okiishi, T., and Copenhaver. W.W., “Stator-Rotor Interactions in a Transonic Compressor, Part 2 Description of a Loss Producing Mechanism,” Accepted for publication in the ASME Journal of Turbomachinery, ASME Turbo Expo, GT-2002-30495, June 2002.

Harff, M. R., Wolff, J. M., Copenhaver, W. W., Car, D., and Estevadeordal, J., "Stator Cascade Flow Vectoring Through Counter Flow Blowing," International Journal of Turbo and Jet Engines, in press. 2003

Harff, M. R., Wolff, J. M., Copenhaver, W. W., Car, D., and Estevadeordal, J., "Stator Cascade Flow Vectoring Through Counter Flow Blowing," International Journal of Turbo and Jet Engines, No. 21, 2004, pp. 155-168.

Harff, M., Wolff, M., Copenhaver, W.W., Car, D., and Estevadeordal, J., 2003 “Stator Cascade Flow Vectoring Through Counter Flow Blowing” Paper Number : AIAA-2003-3408 Session : APA-2 Session Day / Start-Time : 23-Jun-03. Orlando FL.

7.0 REFERENCES

1. Merchant, A., Kerrebrock, J. L., Adamczyk, J. J., and Braunscheidel, E., “ExperimentalInvestigation of a High Pressure Ratio Aspirated Fan stage,” ASME Journal of Turbomachinery, Vol. 127, January 2005, pp. 43–51.

2. Luedke, J., Graziosi, P., Kirtley, K., and Cerretelli, C., “Characterization of Steady Blowing for Flow Control in a Hump Diffuser,” 22nd Applied Aerodynamics Conference and Exhibit, Providence, RI, 2004, AIAA Paper no. 2004-4963.

3. Kirtley, K. R., Graziosi, P., Wood, P., Beacher, B., and Shin, H. W., “Design and Test of an Ultra-Low Solidity Flow-Controlled Stator,” ASME Turbo Expo 2004, Vienna, AU, 2004, ASME Paper no. GT2004-53012.

4. Carter, C. J., Guillot, S. A., Ng, W. F., and Copenhaver, W. W., “Aerodynamic Performance of a High-Turning Compressor Stator with Flow Control,” 37th AIAA/ASME/SAE/ASEE Joint Propulsion Conference & Exhibit, Salt Lake City, UT, 2001, AIAA Paper no. 2001-3973.

5. P.J. Strykowski and A. Krothpalli, “The Countercurrent Mixing Layer, Strategies for Shear-Layer Control,” AIAA Shear Flow Conference, July 6-9, 1993, Orlando, FL

6. P.J. Strykowski, A. Krothapalli and S. Jendoubi, “The Effect of Counterflow on the Development of Compressible Shear Layers”, Journal of Fluid Mechanics, 1996, 308: 63-96

7. M. R. Van der Veer and P. J. Strykowski, “Counterflow Thrust Vector Control of Subsonic Jets: Continuous and Bistable Regimes,” Journal of Propulsion and Power, 1997, Vol. 13, No. 3

8. Car, D., Kuprowicz, N.J., Estevadeordal, J., Zha, G., and Copenhaver, W.W., “Stator Diffusion Enhancement Using a Re-circulating Co-flowing Steady Jet”, ASME Transactions, GT2004-53086, June, 2004.

9. Visbal, M. R., Gaitonde, D. V., and Gogineni, S. P., “Direct Numerical Simulation of a Forced Transitional Plane Wall Jet,” 28th Fluid Dynamics Conference, Snowmass Village, Co, 1998, AIAA Paper no. 1998-2643.

10. Wendt, B. J., “Parametric Study of Vortices Shed from Airfoil Vortex Generators,” AIAA Journal, Vol. 42, No. 11, 2004, pp. 2185–2195.

11. Zha, G., Gao, W., and Paxton, C.D., “Jet Effects on Coflow Jet Airfoil Performance,” AIAA Journal, 2007, Vol 45, No. 6.

12. Car, D., Bailie, S. T., Baudendistel, C. M., Gebbie, D., and Estevadeordal, J., “Fluidic Control Studies for Diffusion Enhancement in Axial Compression Systems,” 44th Aerospace Sciences Meeting and Exhibit, Reno, NV, 2006, AIAA Paper no. 2006-0417.

13. Car, D., Bailie, S. T., Estevadeordal, J., “Slot Jet Flow Control for Diffusion Enhancement: Endwall Observations and Improvements”, 3rd AIAA Flow Control Conference, San Francisco, CA, 2006, AIAA Paper no. 2006-3496.

14. Pearcey, H. H., “Shock Induced Separation and Its Prevention by Design and Boundary Layer Control,” Boundary Layer and Flow Control , edited by G. V. Lachmann, Vol. 2, Pergamon Press Inc., New York, 1961, pp. 1170–1349.

15. Kuethe, A. M. and Chow, C.-Y., **Foundations of Aerodynamics: Bases of Aerodynamic Design**, John Wiley & Sons, 4th ed., 1986.